Deficits in dopaminergic transmission precede neuron loss and dysfunction in a new Parkinson model

Stephanie Janezic[a,b,1], Sarah Threlfell[a,b,1], Paul D. Dodson[a,c,1], Megan J. Dowie[a,c], Tonya N. Taylor[a,b], Dawid Potgieter[a,b], Laura Parkkinen[a,d], Steven L. Senior[a,b], Sabina Anwar[a,b], Brent Ryan[a,b], Thierry Deltheil[a,b], Polina Kosillo[a,b], Milena Cioroch[a,b], Katharina Wagner[a,b], Olaf Ansorge[a,d], David M. Bannerman[a,e], J. Paul Bolam[a,c], Peter J. Magill[a,c], Stephanie J. Cragg[a,b], and Richard Wade-Martins[a,b,2]

[a]Oxford Parkinson's Disease Centre [b]Department of Physiology, Anatomy and Genetics, [c]Medical Research Council Anatomical Neuropharmacology Unit, Department of Pharmacology, [d]Nuffield Department of Clinical Neuroscience, John Radcliffe Hospital, and [e]Department of Experimental Psychology, University of Oxford, Oxford OX1 3QX, United Kingdom

Edited by Thomas C. Südhof, Stanford University School of Medicine, Stanford, CA, and approved September 5, 2013 (received for review May 15, 2013)

The pathological end-state of Parkinson disease is well described from postmortem tissue, but there remains a pressing need to define early functional changes to susceptible neurons and circuits. In particular, mechanisms underlying the vulnerability of the dopamine neurons of the substantia nigra pars compacta (SNc) and the importance of protein aggregation in driving the disease process remain to be determined. To better understand the sequence of events occurring in familial and sporadic Parkinson disease, we generated bacterial artificial chromosome transgenic mice (*SNCA*-OVX) that express wild-type α-synuclein from the complete human *SNCA* locus at disease-relevant levels and display a transgene expression profile that recapitulates that of endogenous α-synuclein. *SNCA*-OVX mice display age-dependent loss of nigrostriatal dopamine neurons and motor impairments characteristic of Parkinson disease. This phenotype is preceded by early deficits in dopamine release from terminals in the dorsal, but not ventral, striatum. Such neurotransmission deficits are not seen at either noradrenergic or serotoninergic terminals. Dopamine release deficits are associated with an altered distribution of vesicles in dopaminergic axons in the dorsal striatum. Aged *SNCA*-OVX mice exhibit reduced firing of SNc dopamine neurons in vivo measured by juxtacellular recording of neurochemically identified neurons. These progressive changes in vulnerable SNc neurons were observed independently of overt protein aggregation, suggesting neurophysiological changes precede, and are not driven by, aggregate formation. This longitudinal phenotyping strategy in *SNCA*-OVX mice thus provides insights into the region-specific neuronal disturbances preceding and accompanying Parkinson disease.

dopamine transmission | in vivo electrophysiology | voltammetry | neurodegeneration | behavioral phenotyping

The development of new disease-modifying therapies for Parkinson disease (PD) is critically dependent on animal models that accurately recapitulate pathophysiological sequelae in an age-dependent manner. The generation of such models using genetically altered animals has proved challenging. The traditional use of heterologous gene promoters in the generation of transgenic mouse models precluded an endogenous transgene expression profile and produced additional phenotypes that are not characteristic of PD (1). In contrast, bacterial artificial chromosome (BAC) technology can enable expression of a desired transgene under the control of its native promoter and regulatory elements to achieve a correct spatiotemporal expression profile, thereby providing a more physiological model for investigating molecular mechanisms of the disease.

The α-synuclein gene (*SNCA*) has been implicated in PD through three dominant point mutations (2–4) and locus multiplication (5, 6). *SNCA* duplications and triplications cause autosomal-dominant PD in which the age of onset and disease severity are related in a gene dosage-dependent manner (5, 6). More recently, genome-wide association studies (GWASs) have demonstrated a link between common *SNCA* variants and sporadic forms of PD, with disease-associated polymorphisms proposed to increase α-synuclein (α-syn) expression either by increasing transcription or stabilizing mRNA (7–9). Although α-syn aggregation into cytoplasmic Lewy bodies is seen in human PD patient postmortem tissue, it is not known whether neurophysiological dysfunction and cell death precede the formation of aggregates.

To better understand the mechanisms by which elevated α-syn leads to the progressive neuronal dysfunction seen in PD, we have generated BAC transgenic mice (*SNCA*-OVX) that express human wild-type α-syn at twice the endogenous level of mouse α-syn. Using a longitudinal "deep phenotyping" strategy in these *SNCA*-OVX mice, in vitro and in vivo, we find disturbances to midbrain dopamine neuron function at discrete phases that precede and/or accompany PD-like loss of dopamine neurons and motor deficits. Specifically, dopamine transmission and vesicular organization are compromised selectively in dorsal striatum before a subsequent loss of dopamine neurons, abnormal firing in remaining dopamine neurons in vivo, and movement deficits. These findings thus provide key insights into the progression of events in PD.

Results

Molecular Characterization of *SNCA*-OVX Mice. We generated *SNCA* transgenic mice using a BAC construct carrying the complete

Significance

Elevated expression of the presynaptic protein α-synuclein underlies familial and sporadic Parkinson disease (PD). However, our understanding of how increases in α-synuclein levels drive the sequence of events leading to PD is incomplete. Here, we apply a multidisciplinary longitudinal analysis to a new α-synuclein transgenic mouse model. We show that early-stage decreases in dopamine release and vesicle reclustering precede late-stage changes in neuronal firing properties, measured by in vivo recordings from vulnerable neurons. Accumulated deficits in dopamine neurotransmission and altered neuronal firing are associated with cell death and motor abnormalities, in the absence of protein aggregation in the substantia nigra. These findings have important implications for developing therapies.

Author contributions: O.A., D.M.B., J.P.B., P.J.M., S.J.C., and R.W.-M. designed research; S.J., S.T., P.D.D., M.J.D., T.N.T., D.P., L.P., S.L.S., S.A., B.R., T.D., P.K., M.C., and K.W. performed research; S.J., S.T., P.D.D., M.J.D., T.N.T., D.P., L.P., B.R., T.D., D.M.B., J.P.B., P.J.M., S.J.C., and R.W.-M. analyzed data; and S.J., S.T., P.D.D., J.P.B., P.J.M., S.J.C., and R.W.-M. wrote the paper.

The authors declare no conflict of interest.

This article is a PNAS Direct Submission.

Freely available online through the PNAS open access option.

[1]S.J., S.T., and P.D.D. contributed equally to this work.

[2]To whom correspondence should be addressed. E-mail: richard.wade-martins@dpag.ox.ac.uk.

This article contains supporting information online at www.pnas.org/lookup/suppl/doi:10.1073/pnas.1309143110/-/DCSupplemental.

111-kb wild-type human *SNCA* locus (Fig. S1*A*). Two mouse lines were generated: *SNCA*-OVX, which overexpresses human α-syn to levels that model those associated with *SNCA* multiplications (10), and hα-syn, which expresses human α-syn at a low/moderate level as a control for expression of human α-syn. Both lines were bred to a mouse α-syn-null ($Snca^{-/-}$) pure C57/Bl6 background (11) to preclude confounding interactions with endogenous α-syn. Complete transgene integration was confirmed by exon PCR amplification of all six human *SNCA* exons (Fig. S1*B*). For *SNCA*-OVX mice, a single site of integration was identified by

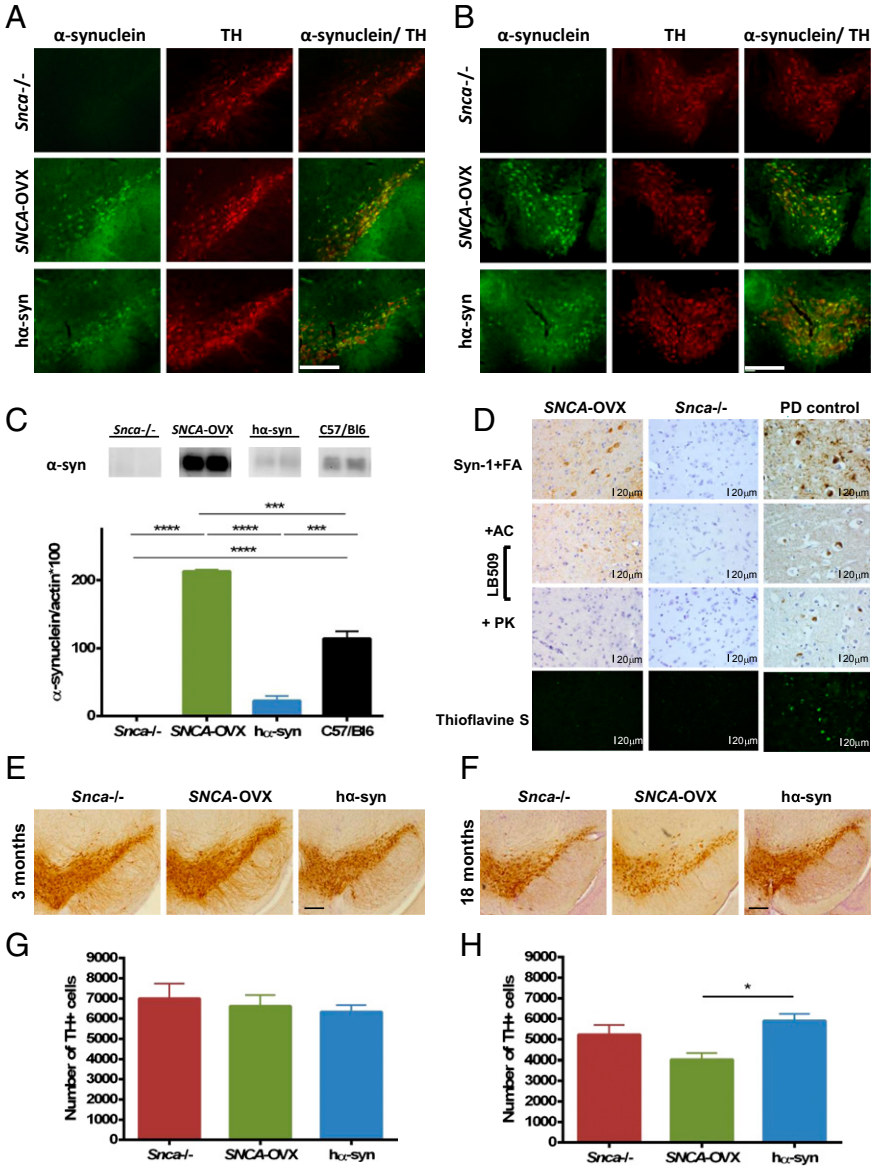

Fig. 1. Characterization of α-syn transgenic mice. (*A and B*) Double immunofluorescence labeling for α-syn and TH confirms human α-syn transgene expression in TH-immunoreactive dopamine neurons of the (*A*) SNc and (*B*) VTA in 3-mo-old *SNCA*-OVX and hα-syn animals. (Scale bars, 200 μm.) (*C*) Quantitative Western analysis of striatal α-syn expression in 3-mo-old *SNCA*-OVX, hα-syn, $Snca^{-/-}$, and C57/Bl6 animals reveals that *SNCA*-OVX animals express the human wild-type *SNCA* transgene at 1.9-fold higher levels compared with endogenous mouse α-syn protein in C57/Bl6 animals. No α-syn expression was observed in $Snca^{-/-}$ control animals. One-way ANOVA with Bonferroni post hoc analysis; $^{****}P < 0.0001$, $^{***}P < 0.001$, $n = 2$–3. (*D*) Immunohistochemical analysis revealed somatic cytoplasmic α-syn immunostaining in cells of the SNc in 18-mo-old *SNCA*-OVX mice using the Syn-1 antibody with formic acid (FA) pretreatment. Similar structures were weakly labeled in 18-mo-old *SNCA*-OVX mice using the LB509 antibody autoclaved (AC) in citric buffer. This staining was abolished when proteinase K (PK) antigen retrieval was applied instead. All of these immunohistochemical stainings were carried out together with control tissue (entorhinal cortex from a PD patient with dementia that shows prominent Lewy body and neuritic pathology). No "amyloid" pathology was detected with thioflavine S in either 18-mo-old *SNCA*-OVX or $Snca^{-/-}$, whereas several Lewy bodies and dystrophic neurites were detected in the positive PD control. (Scale bars, 20 μm; magnification: all pictures, 400×.) (*E* and *G*) At 3 mo of age, stereological cell counting revealed no differences in the number of TH-immunoreactive neurons in the SNc of *SNCA*-OVX mice compared with hα-syn and $Snca^{-/-}$ mice. One-way ANOVA: no main effect of genotype: $F < 1$, $P > 0.05$, $n = 5$ per genotype. Data are expressed as the mean ± SEM. Representative images of TH-immunoreactivity in the SNc are shown. (Scale bar, 200 μm.) (*F* and *H*) Analysis of 18-mo-old animals revealed a 30% loss of TH-immunoreactive neurons in the SNc of *SNCA*-OVX mice compared with hα-syn mice. One-way ANOVA with Bonferroni post hoc analysis: main effect of genotype: $F_{(2,12)} = 6.3$, $^{*}P < 0.05$, $n = 5$ per genotype. Data are expressed as the mean ± SEM. Representative images of TH immunoreactivity in the SNc are shown. (Scale bar, 200 μm.)

fluorescence in situ hybridization analysis near the centromere of chromosome 4 and, for hα-syn mice, a single site near the telomere of chromosome 2 (Fig. S1*C*).

Double immunofluorescence labeling for tyrosine hydroxylase (TH) and α-syn revealed transgene expression in TH-immunoreactive dopamine neurons in the substantia nigra pars compacta (SNc) (Fig. 1*A*) and ventral tegmental area (VTA) (Fig. 1*B*) of *SNCA*-OVX and hα-syn (but not *Snca*$^{-/-}$) mice. Transgene expression was also found to recapitulate the regional expression pattern of endogenous mouse α-syn in other brain regions including cortex, hippocampus, and striatum (Fig. S1*E*). Human α-syn levels in the striatum of *SNCA*-OVX mice were 1.9-fold higher relative to the levels of endogenous mouse α-syn in age-matched C57/Bl6 animals (Fig. 1*C*). We observed no change in β-synuclein or γ-synuclein levels in *SNCA*-OVX mice (Fig. S1*D*).

Soluble high-molecular-weight α-syn species were observed in the midbrain of *SNCA*-OVX mice at both 3 and 18 mo of age, but not in hα-syn mice, as assessed by native PAGE (Fig. S2*A*). The absence of soluble high-molecular-weight species in hα-syn mice was confirmed by loading increasing amounts of protein, such that the levels of α-syn in the samples were comparable, without the appearance of the smear of higher-molecular-weight species being seen. In addition, it was confirmed that these soluble species were similar to those observed in PD, by comparison with SNc tissue from a PD patient. A C-terminal truncated form of α-syn was observed at low levels in the midbrain of 18-mo-old *SNCA*-OVX mice, as demonstrated by Western blotting with an antibody raised against the central portion (aa 18–123) of α-syn followed by reprobing with an antibody raised against the C terminus (aa 118–123) of α-syn (Fig. S2*B*). This truncation generated a fragment comparable in size to that observed in the SNc of a PD patient but was not observed in hα-syn mice or in any of the samples probed with the C-terminal antibody. No evidence of α-syn phosphorylation at S129 was observed in any of the mice strains using a number of commercial S129P antibodies (Fig. S2*C*).

We looked for the presence of pathological α-syn aggregates in the *SNCA-OVX* line at 18 mo of age. Proteinase K treatment, which enhances the immunoreactivity of "abnormal" α-syn (i.e., that in intracytoplasmic aggregates) and also diminishes that of diffuse physiological expression (12), abolished the immunoreactivity of α-syn in the SNc (Fig. 1*D*) and striatum (Fig. S3*A*) of aged *SNCA*-OVX mice. Similarly, thioflavine S, which detects the β-sheet–rich amyloid and p62, a common constituent in several types of disease-associated inclusions, revealed no pathological protein aggregations in the SNc of *SNCA*-OVX mice (Fig. S3*B*). No qualitative differences in astrogliosis or microglial activation were detected between *SNCA*-OVX mice and *Snca*$^{-/-}$ controls, as analyzed by immunohistochemistry using antibodies against GFAP and Iba-1, respectively (Fig. S3*B*). Hyperphosphorylated tau (AT8) and β-amyloid (4G8) staining was negative in all animals (Fig. S3*B*).

Aged *SNCA*-OVX Animals Lose Nigrostriatal Dopamine Neurons. To assess whether progressive degeneration of SNc dopamine neurons, a cardinal pathological feature of PD, occurs as a consequence of overexpressing α-syn, an unbiased stereological count of TH-immunoreactive neurons was performed in the SNc of 3- and 18-mo-old mice. It is already known that *Snca*$^{-/-}$ mice display a small decrease in dopamine neurons (13, 14); therefore, to evaluate the effects of increased levels of α-syn we compared the number of dopamine neurons in *SNCA*-OVX to those in hα-syn mice. In young adults (3 mo), no difference was found in the number of TH-immunoreactive neurons between genotypes (Fig. 1 *E* and *G*). However, in aged mice (18 mo), *SNCA*-OVX animals displayed a 30% reduction in TH-immunoreactive neurons in the SNc compared with the hα-syn mice (Fig. 1 *F* and *H*). At 18 mo of age, *SNCA*-OVX animals also displayed a 22% reduction in hematoxylin-counterstained neurons in the SNc compared with the hα-syn mice (Fig. S4*B*), whereas no difference in hematoxylin-stained cells was observed at 3 mo of age (Fig. S4*A*), confirming that the loss of TH-immunoreactive neurons in aged *SNCA*-OVX mice was not due to a down-regulation of TH expression. The loss of SNc dopamine neurons in aged *SNCA*-OVX mice was observed in the absence of overt aggregation pathology in the SNc and striatum, suggesting α-syn aggregation is not required for neuronal death in the SNc.

SNCA-OVX Mice Display Early Nonmotor and Late Motor Phenotypes. *SNCA*-OVX and control mice were analyzed for nonmotor phenotypes that reflect early symptoms of PD. We assessed gastrointestinal function and revealed an increased dry stool weight in male *SNCA*-OVX mice that was independent of age (Fig. 2*A*). This increase in dry stool weight was not accompanied by an increased stool frequency or stool water content (Fig. S5 *A* and *B*), indicating a constipation-like phenotype that was seen in male, but not female, *SNCA*-OVX mice.

We next assessed motor function using the accelerating rotarod, multiple static rods, and the forepaw stride length tests. On the rotarod test, the latency of aged (18 mo) but not young (3 mo) *SNCA*-OVX mice to fall was significantly reduced compared with hα-syn and *Snca*$^{-/-}$ controls (Fig. 2*B*). *SNCA*-OVX animals at 18 mo of age were also impaired on the multiple static rods test (Fig. 2 *C–E* and Movies S1 and S2) compared with age-matched controls. *SNCA*-OVX mice also displayed a reduced forepaw stride length compared with littermate control *Snca*$^{-/-}$ mice (Fig. 2*F*). *SNCA*-OVX mice did not display differences in latency to fall in the inverted screen test compared with age-matched hα-syn and *Snca*$^{-/-}$ controls, indicating that poor performance in the rotarod and multiple static rods tests was due to impaired motor coordination rather than muscle weakness (Fig. S5*C*).

Early and Sustained Deficits in Dopamine Transmission in the Dorsal Striatum of *SNCA*-OVX Mice. Having established a mouse model that displays an age-dependent Parkinsonian phenotype, we sought to investigate what changes might precede or accompany the phenotypic alterations. In PD, the nigrostriatal dopamine neurons projecting from the SNc to the dorsal striatum [caudate putamen (CPu)], are preferentially affected compared with mesolimbic dopamine neurons projecting from the VTA to the ventral striatum [nucleus accumbens (NAc)]. Expression of the α-syn transgene was confirmed in both the CPu and NAc of *SNCA*-OVX transgenic mice (Fig. S6 *A* and *B*). To investigate region- and age-dependent changes in dopamine transmission in *SNCA*-OVX mice, we used fast-scan cyclic voltammetry (FCV) at carbon-fiber microelectrodes, which detects dopamine release and reuptake in real time. In the dorsal striatum, mean peak extracellular concentrations of dopamine ($[dopamine]_o$) evoked by single electrical pulses across distributed recording sites were, on average, ∼30% lower in *SNCA*-OVX mice than in littermate *Snca*$^{-/-}$ controls (Fig. 3 *A–C*, left traces). This reduced release was present from a young age (3–4 mo) before the loss of dopamine neurons (Fig. 1*H*) and persisted throughout the lifespan of adult mice (tested at 3–4, 12, and 18 mo). The greatest deficits were found in dorsal and lateral recording sites (Fig. 3*G*). In contrast, in the ventral striatum no significant difference in evoked $[dopamine]_o$ was detected between the two genotypes at any time point (Fig. 3 *A–C*, right traces).

In young and aged hα-syn mice, mean peak $[dopamine]_o$ evoked by single pulses in CPu or NAc was not significantly different from that in *Snca*$^{-/-}$ littermates (Fig. 3 *H* and *I*), suggesting that the deficit in evoked $[dopamine]_o$ in *SNCA*-OVX mice was a consequence of the elevated levels of human α-syn rather than its expression per se. Dopamine content of CPu or

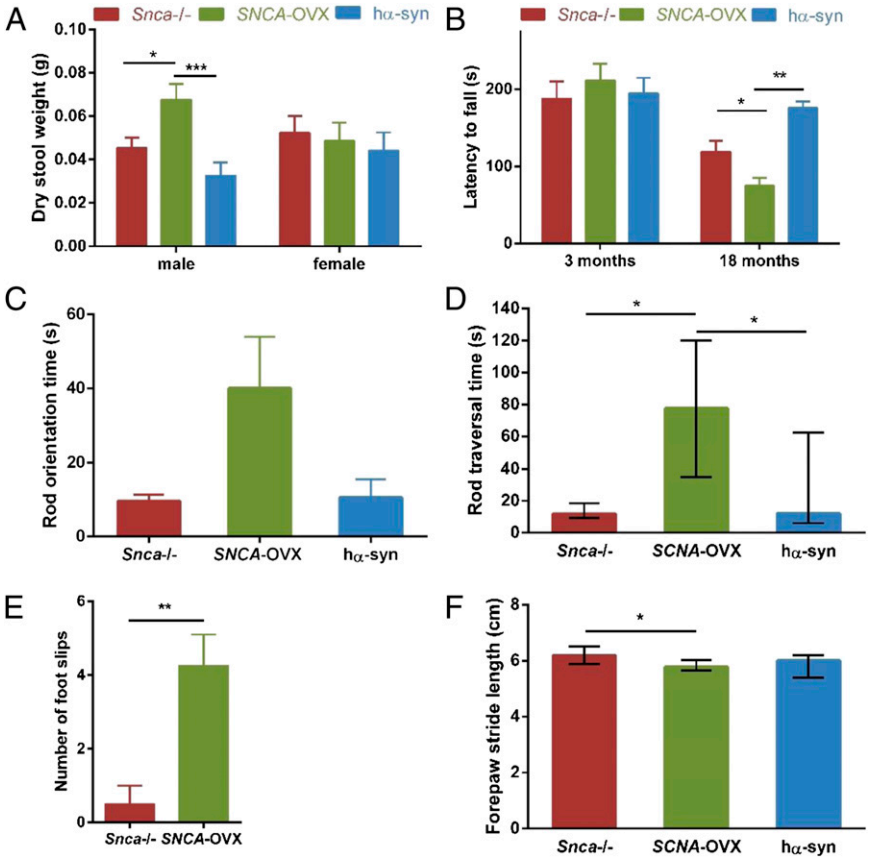

Fig. 2. Early nonmotor and late motor phenotypes in *SCNA*-OVX mice. (*A*) Male *SNCA*-OVX animals displayed an increased dry stool weight independent of age. Three-way ANOVA; main effect of age: $F_{(1,84)} = 20.66$, $^{****}P < 0.0001$; genotype/sex interaction: $F_{(2,83)} = 3.19$, $^{*}P < 0.05$; no interaction between genotype and age: $F_{(2,83)} = 1.44$, $P > 0.05$; separate ANOVA for males: main effect of genotype: $F_{(2,45)} = 7.76$, $^{***}P < 0.001$ (Tukey post hoc test $^{*}P < 0.05$, $^{***}P < 0.001$), $n = 4$–11; females: main effect of genotype: $F < 1$, $P > 0.05$, $n = 3$–8. Data are expressed as mean ± SEM. (*B*) Rotarod performance was impaired in 18- but not in 3-mo-old *SNCA*-OVX mice. Two-way ANOVA of square-root transformed data: main effect of age: $F_{(1,28)} = 25.95$, $^{***}P < 0.001$; main effect of genotype: $F_{(2,27)} = 3.49$, $^{*}P < 0.05$; genotype/age interaction: $F_{(2,27)} = 6.14$, $^{**}P < 0.01$; separate ANOVAs revealed no main effect of genotype at 3 mo ($F < 1$, $P > 0.05$), but a significant main effect of genotype at 18 mo ($F_{(2,15)} = 10.04$, $^{**}P < 0.01$) (Tukey post hoc test $^{*}P < 0.05$, $^{**}P < 0.01$), $n = 3$–8), which remained significant when body weight was included as a covariate (ANCOVA: main effect of genotype: $F_{(2,14)} = 4.93$, $^{*}P < 0.05$). Data are expressed as mean ± SEM. (*C*–*E*) *SNCA*-OVX animals (18 mo old) were impaired on the multiple static rods test compared with hα-syn and *Snca*$^{-/-}$ animals. (*C*) Orientation: ANOVA of square-root transformed data collapsed across both rods; main effect of genotype: $F_{(2,24)} = 3.35$, $P = 0.05$, $n = 7$–10. Data are expressed as mean ± SEM. (*D*) Traversing: Kruskal–Wallis one-way ANOVA on ranked data collapsed across both rods. Effect of genotype: $H_2 = 12.37$; $^{**}P < 0.01$ (Dunn's post hoc pairwise comparison $^{*}P < 0.05$), $n = 7$–10. Data are expressed as median ± IQ range. (*E*) *SNCA*-OVX animals displayed increased foot slips when traversing rod 2 ($^{**}P < 0.01$, Welch *t* test: $t = 3.79$, df = 6, $n = 4$ per group). Rods had a diameter of 22 mm (rod 1) and 9 mm (rod 2). (*F*) *SNCA*-OVX animals displayed reduced stride length compared with *Snca*$^{-/-}$ mice (Kruskal–Wallis one-way ANOVA on ranked data, comprising data from both ages and sexes: main effect of genotype: $H_{(2)} = 10.79$, $^{**}P < 0.01$ (Dunn's post hoc pairwise comparison $^{*}P < 0.05$), $n = 15$–30). Data are expressed as median ± IQ range.

NAc assessed by HPLC was not significantly different between hα-syn and *Snca*$^{-/-}$ mice at either 3 or 18 mo (Fig. 3 *J* and *K*). Because no phenotypic changes were detected in hα-syn mice compared with *Snca*$^{-/-}$ mice, our subsequent analyses focused on comparing *SNCA*-OVX transgenic mice with their littermate control *Snca*$^{-/-}$ mice.

Lower levels of evoked $[\text{dopamine}]_o$ in dorsal striatum of *SNCA*-OVX compared with *Snca*$^{-/-}$ mice were not due to reduced striatal dopamine content: HPLC analysis showed net dopamine content was unchanged in CPu or NAc in *SNCA*-OVX compared with *Snca*$^{-/-}$ mice at 3–4 and 12 mo (Fig. 3 *D* and *E*), whereas at 18 mo dopamine content in CPu (but not NAc) was, paradoxically, greater in *SNCA*-OVX mice compared with *Snca*$^{-/-}$ controls, and unaltered in NAc (Fig. 3*F*). Furthermore, apparent deficits in dopamine release in dorsal CPu of either young or aged adult *SNCA*-OVX mice were not due to diminished $[\text{dopamine}]_o$ that might result from enhanced dopamine uptake, because dopamine uptake kinetics were normal (Fig. S6*C*). No change in the level of dopamine transporter protein was observed (Fig. S6*D*). In addition, we excluded a role for striatal ACh input to dopamine axons from cholinergic interneurons, which play a key role in driving dopamine release probability (15): A dopamine release deficit persisted in the presence of nicotinic receptor blockade by dihydro-β-erythroidine (Fig. S6 *E* and *F*). There were also no detectable changes in the net dependence on extracellular Ca^{2+} (Fig. S6*G*).

No Change in SNARE Complex Formation but Changes in Dopamine Vesicle Distribution. We next sought to understand the underlying molecular, neuroanatomical, and neurophysiological changes in the SNc that may lead to progressive neuronal loss in the *SNCA*-OVX model of PD. The reduction in evoked $[\text{dopamine}]_o$ seen before loss of dopamine neurons or dopamine content suggests a reduction in the releasability of dopamine. However, we found no differences in SNARE complex formation in the striatum of 6-mo-old *SNCA*-OVX mice compared with age-matched controls (Fig. S7 *A* and *B*) or any changes in the striatal protein levels of SNAP25, VAMP2, complexins, or synapsins (Fig. S7 *C*–*G*). These

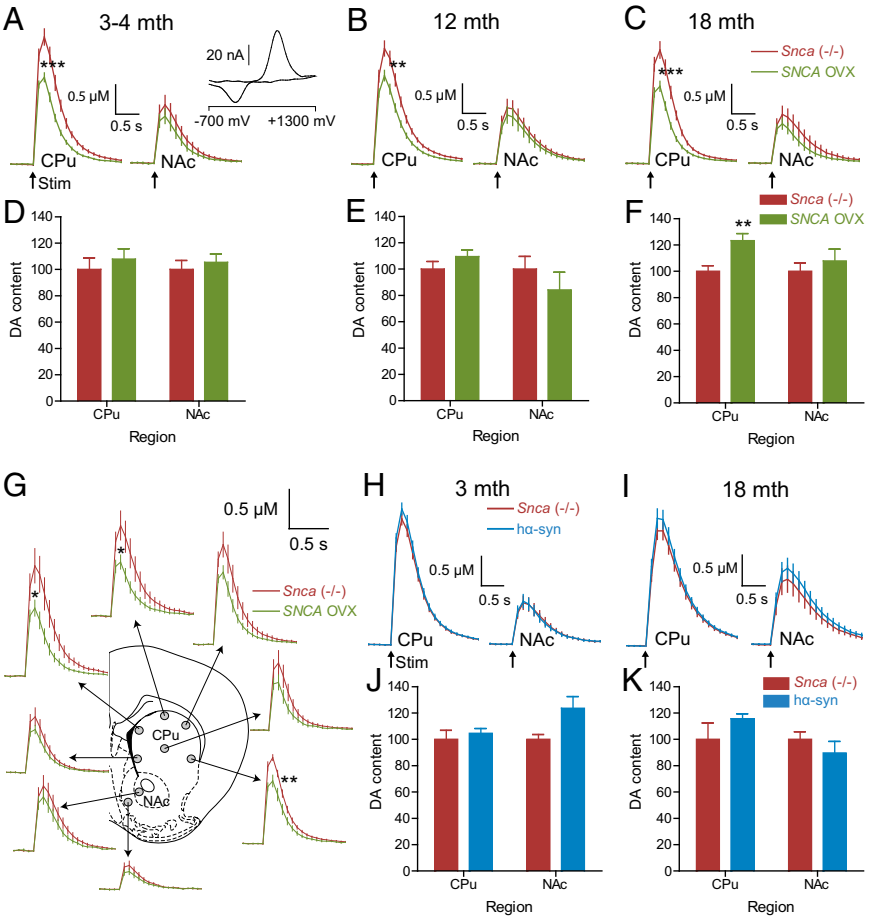

Fig. 3. α-syn overexpression limits dopamine release from an early age in CPu, but not NAc. (*A–C*) Mean extracellular dopamine concentration ($[dopamine]_o$) profiles vs. time (mean ± SEM) following single pulse stimulation (↑200 μs, 0.6 mA) in CPu (*A–C*, left traces) or NAc (*A–C*, right traces) of *Snca*$^{-/-}$ vs. *SNCA*-OVX at increasing ages. Mean peak evoked $[dopamine]_o$ was significantly lower in *SNCA*-OVX compared with *Snca*$^{-/-}$ in CPu (**$P < 0.01$, ***$P < 0.001$; unpaired *t* test; $n = 60–72$) but not NAc ($P > 0.05$; unpaired *t* test; $n = 19–23$) at 3–18 mo. (*D–F*) Dopamine content (expressed as a percentage of *Snca*$^{-/-}$) in CPu and NAc dissected from striatal slices used for FCV recordings. Mean dopamine content was not significantly different between *SNCA*-OVX and *Snca*$^{-/-}$ in CPu or NAc ($P > 0.05$, unpaired *t* test, $n = 10$) between ages 3 and 12 mo. However, at 18 mo mean dopamine content was significantly greater in CPu of *SNCA*-OVX compared with *Snca*$^{-/-}$ (*F*; **$P < 0.01$, unpaired *t* test, $n = 12$) but not NAc. (*G*) Typical FCV recording sites include six CPu and two NAc recordings. Mean peak $[dopamine]_o$ from individual sites from 3- to 4-mo-old *Snca*$^{-/-}$ and *SNCA*-OVX highlights more prominent $[dopamine]_o$ deficit in dorsal striatum (ventrolateral striatum **$P < 0.01$; dorsomedial and dorso-mid striatum *$P < 0.05$; all other regions $P > 0.05$; unpaired *t* test; $n = 10–14$ per region). (*H* and *I*) The hα-syn mice show no difference compared with *Snca*$^{-/-}$ mice in mean peak evoked $[dopamine]_o$ ($P > 0.05$; unpaired *t* test; *H*: 3 mo, $n = 18$ NAc, $n = 60$ CPu; *I*: 18 mo, $n = 15$ NAc, $n = 47$ CPu) or dopamine content ($P > 0.05$; unpaired *t* test; *J*: 3 mo, $n = 10$; *K*: 18 mo, $n = 7$) in CPu or NAc. Absolute values for dopamine content ranged from 97 to 240 pmol/mm^3 tissue in CPu to 47–104 pmol/mm^3 tissue in NAc.

results are consistent with previous finding that striatal SNARE complex formation in striatum is not regulated by synucleins (16).

We next explored the alternative hypothesis that α-syn might restrict dopamine release by altering the distribution of the vesicular pool in dopamine axons in the dorsal striatum (17). We used electron microscopy to analyze the structure of TH-immunoreactive synaptic and nonsynaptic axonal profiles in the CPu of 3-mo-old *SNCA*-OVX and *Snca*$^{-/-}$ mice. The mean cross-sectional area of profiles, the number and density of vesicles per profile, and the distance of vesicles to the plasma membrane were similar in both genotypes (Table S1). When a synapse was present, there were also no differences in the synaptic membrane length or distance of vesicles to the active zone. However, vesicles in *SNCA*-OVX mice were more clustered than those in *Snca*$^{-/-}$ mice; the frequency distribution of intervesicle distance was significantly different between genotypes ($P < 0.0001$; two-sample Kolmogorov–Smirnov test; Fig. 4), and vesicles were three times less dispersed in *SNCA*-OVX mice (index of dispersion $D_{SNCA\text{-}OVX}/D_{Snca}{}^{-/-} = 0.34$).

Monoamine Neurotransmission Deficit Does Not Extend to Norepinephrine or 5-Hydroxytryptamine. To determine whether the deficit in dopamine release in the dorsal striatum of *SNCA*-OVX mice is seen for other amines elsewhere, we investigated the release of norepinephrine (NE) and 5-hydroxytryptamine (5-HT) from axon terminals in innervation-rich areas, the bed nucleus of the stria terminalis (BNST) and substantia nigra pars reticulata (SNr), respectively. We confirmed transgene expression in the cell soma regions, the locus coeruleus and the dorsal raphe nucleus, in *SNCA*-OVX mice by immunohistochemistry (Fig. S8). Mean peak extracellular concentrations of NE ($[NE]_o$) in the ventromedial portion of the BNST (Fig. 5 *A* and *B*) evoked by stimulus trains of 30 pulses at 10, 25, 50, and 100 Hz in *SNCA*-OVX mice were not different from those in *Snca*$^{-/-}$ mice irrespective of age (3 or 18 mo; Fig. 5 *C–F*). Similarly, mean peak extracellular concentrations of 5-HT ($[5\text{-}HT]_o$) in SNr (Fig. 5 *G* and *H*) evoked by stimulus trains of 20 or 40 pulses at 50 Hz in *SNCA*-OVX mice were not different from those in *Snca*$^{-/-}$ mice at either young (3 mo, Fig. 5 *I* and *J*) or old age (18 mo, Fig. 5 *K* and *L*). These data show that α-syn overexpression does not

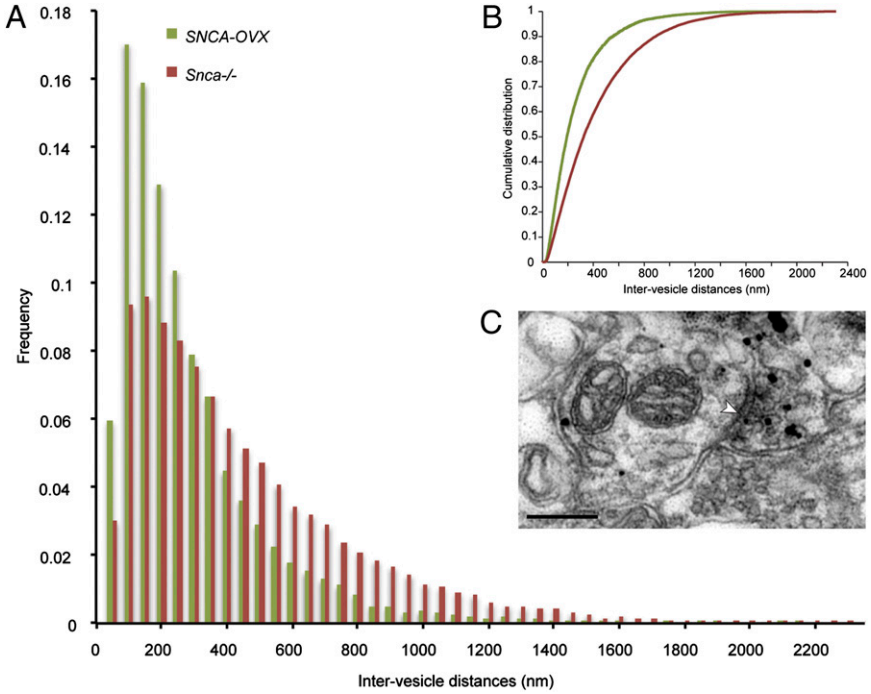

Fig. 4. Overexpression of α-syn alters vesicle clustering in dopaminergic synaptic boutons in the dorsal striatum. (*A*) Frequency distribution of intervesicle distance in TH-immunoreactive profiles in the striatum of *SNCA-OVX* and $Snca^{-/-}$ mice. The two-sample Kolmogorov–Smirnov test was performed to test for differences between the two distributions and revealed a significant difference between the groups (****$P < 0.0001$). (*B*) Cumulative distribution functions of the two data groups. Application of an index of dispersion, $D = \sigma^2/\mu$, to each raw dataset ($D_{SNCA\text{-}OVX}$, $D_{Snca^{-/-}}$) shows that the $Snca^{-/-}$ vesicles are three times more dispersed than the *SNCA-OVX* ($D_{SNCA\text{-}OVX}/D_{Snca^{-/-}} = 0.34$). (*C*) Electron micrograph of a TH immunogold-labeled axon terminal in the dorsal striatum identified by the accumulation of electron dense silver-intensified immunogold particles. The bouton forms symmetrical synaptic contact (arrowhead) with a dendritic shaft. Note the accumulation of vesicles within the bouton. (Scale bar, 0.2 μm.)

affect the axonal release of 5-HT or NE, further suggesting that the neurotransmission deficit in *SNCA*-OVX mice is highly selective for cell type and brain circuit.

SNc Dopamine Neurons in *SNCA*-OVX Mice Exhibit Age-Dependent Reductions in Firing Rates in Vivo. To gain further insight into the pathophysiological sequelae of α-syn overexpression in midbrain dopamine systems, we tested for changes in the action potential firing properties of SNc dopamine neurons in vivo. We made extracellular recordings from individual SNc neurons in young and aged (3–4 and 18–22 mo) anesthetized *SNCA*-OVX mice and their $Snca^{-/-}$ littermates (Fig. 6). After recording, we juxtacellularly labeled each neuron with Neurobiotin (18) to confirm its dopamine phenotype (TH immunoreactivity) and location in SNc, as well as test for their expression of α-syn (Fig. 6 *A* and *C*; all recorded dopamine neurons ($n = 43$) from *SNCA*-OVX mice expressed the α-syn transgene). In young *SNCA*-OVX and $Snca^{-/-}$ mice, the firing rates and action potential durations of SNc dopamine neurons were similar (Fig. 6*E*). Moreover, neurons in both genotypes exhibited similar coefficients of variation (a measure of regularity of firing) and propensities to fire in a "regular," "irregular," or "bursty" pattern (Fig. 6*G* and *SI Materials and Methods*). Thus, in young adult animals at least, α-syn overexpression does not alter these key firing properties of SNc dopamine neurons. However, for SNc dopamine neurons recorded in the aged *SNCA*-OVX and $Snca^{-/-}$ mice (Fig. 6 *B* and *D*), we found a significant reduction (nearly 30%) in the firing rate, but no change in the firing patterns, of dopamine neurons in *SNCA*-OVX mice (Fig. 6 *F* and *H*). Taken together, these data show that overexpression of human α-syn does not compromise key firing properties of SNc dopamine neurons in young adulthood but significantly reduces the firing rates of these neurons in old age.

Discussion

Here, we describe the generation and longitudinal deep-phenotyping of a unique transgenic model of PD and identify the sequence of disease mechanisms triggered by overexpression of α-syn to levels associated with both familial and sporadic human disease. Using transgenic *SNCA*-OVX mice, we have localized early and selective deficits in dopamine neurotransmission to the nigrostriatal pathway. This early-onset phenotype is followed in aged animals by a pathology of loss of dopamine neurons, reduced SNc dopamine neuron firing rates, and motor impairments. Furthermore, this constellation of Parkinsonian phenotypes caused by elevated α-syn is not dependent on overt protein aggregation but is associated with soluble high-molecular-weight α-syn species observed at 3 and 18 mo of age in *SNCA*-OVX mice.

Our use of BAC transgenesis to overexpress human wild-type α-syn from the complete human genomic DNA locus driven by the endogenous promoter helped ensure correct spatiotemporal regulation of expression, reflecting endogenous α-syn expression. Overexpression of α-syn is a likely mechanism underlying both rare familial PD, caused by *SNCA* duplications and triplications (5, 6), and sporadic PD (19). PD-associated variants at the *SNCA* locus, identified by GWAS, are proposed to enhance expression by either increasing *SNCA* transcription or enhancing mRNA stability (9). The *SNCA*-OVX mouse therefore acts as a model of both familial and sporadic PD. The *SNCA*-OVX line expresses the *SNCA* transgene at 1.9-fold the levels of endogenous mouse α-syn; this near-doubling mirrors the change in human α-syn levels that result from a triplication of the *SNCA* locus in familial PD (10). Elevated levels of α-syn have previously also been demonstrated in sporadic cases of PD in which remaining dopamine midbrain neurons from patients with sporadic disease show up to a sixfold increase in α-syn mRNA levels (19).

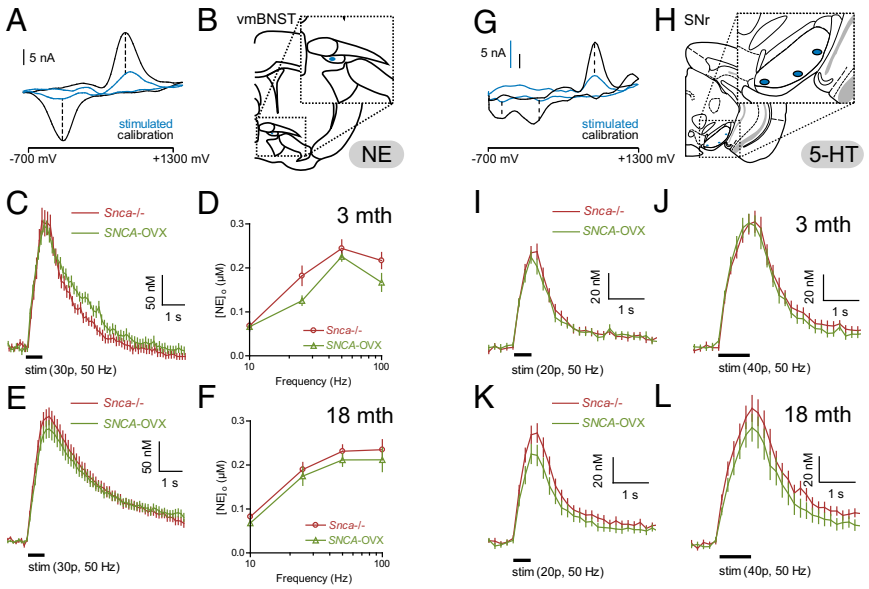

Fig. 5. α-syn overexpression does not alter nondopamine amine signaling in bed nucleus of the stria terminalis and substantia nigra pars reticulata. (*A*) Typical cyclic voltammograms from electrically evoked recordings of NE in BNST (stimulated) and following calibration in 2 μM NE (calibration). Note single oxidation and reduction current peaks at +560–580 and −200 mV, respectively. (*B*) Typical recording site in ventromedial portion of BNST (vmBNST) ∼0.26 mm anterior of bregma. Mean profiles of extracellular NE concentration ($[NE]_o$) vs. time (mean ± SEM) following train stimulation (30 pulses, 50 Hz) in vmBNST in young adult (*C*) (3 mo, n = 33–35) or aged adult (*E*) (18 mo, n = 70–74) *Snca*$^{-/-}$ vs. *SNCA*-OVX mice. Mean peak $[NE]_o$ vs. frequency during 30 pulse trains (10–100 Hz) in vmBNST in young adult (*D*) (n = 33–35) or aged adult (*F*) (n = 70–74). (*G*) Typical cyclic voltammograms from electrically evoked recordings of 5-HT in SNr (stimulated) and following calibration in 0.5 μM 5-HT (calibration). Note single oxidation and dual reduction current peaks at approximately +600, −20, and −670 mV, respectively. (*H*) Typical recording sites in the SNr ∼3.2 mm posterior of bregma. Note recording sites located on ventral side of SNr to minimize any possible contribution of dendritic dopamine in recordings. Mean profiles of $[5\text{-HT}]_o$ vs. time following 50-Hz train stimulation (*I*: 20 pulses or *J*: 40 pulses; n = 31–44) in the SNr in young adult (3 mo) and aged adult (18 mo) (*K*: 20 pulses or *L*: 40 pulses; n = 26–32) *Snca*$^{-/-}$ vs. *SNCA*-OVX mice.

Our study is unique in defining the effect of disease-relevant α-syn overexpression on neurotransmission and vesicle organization in the dopamine pathways most vulnerable in PD. We find an early and sustained deficit in neurotransmission specific to dopamine (rather than the other monoamines, NE and 5-HT). Furthermore, this deficit was localized to the dopamine inputs to dorsal striatum. These findings are reminiscent of our previous work on α-and γ-synuclein double-knockout and α-, β-, γ-synuclein triple-knockout mice, in which we showed that synucleins negatively regulate dopamine release in the dorsal but not ventral striatum (16, 20).

At time points before 18 mo of age, we observed no change in striatal dopamine content, despite a decrease in release. This is consistent with a redistribution, rather than a reduction, of dopamine at release sites. In support of this, we identified increased clustering of vesicles in dopamine terminals in the dorsal striatum of *SNCA*-OVX animals at 3 mo.

Whether the in vivo firing properties of SNc dopamine neurons change before protein aggregation and/or cell death has been a critical, unaddressed issue in PD. We show here that the activity of neurochemically identified SNc dopamine neurons is altered in an age- and genotype-dependent manner. Because midbrain dopamine neurons collectively innervate all basal ganglia nuclei (21), any change in their firing rate or pattern is likely to profoundly disturb the activity of the whole basal ganglia network; it is these disturbances that ultimately underlie the motor symptoms of PD. We found that the spontaneous firing rates of SNc dopamine neurons were reduced by nearly 30% in aged animals overexpressing α-syn. This decrease in spontaneous firing rates, together with dopamine neuron loss and a sustained deficit in striatal dopamine release, may collectively tip the balance toward a greatly reduced dopamine output that can no longer be compensated for, thus resulting in motor impairments in aged animals. It is not clear whether the reduced firing rates of dopamine neurons are a response to alterations in either their inputs or intrinsic properties, or whether this change is, in itself, pathogenic.

The age-related, progressive loss of nigrostriatal dopamine neurons and the presence of α-syn–containing Lewy bodies are the cardinal features of PD pathology. However, the precise relationship between α-syn pathology and dopamine neuron dysfunction and death has been unclear. We show here that dopamine neuronal dysfunction and neuronal death in *SNCA*-OVX mice occurs in the absence of overt protein aggregation pathology in the SNc and striatum but is associated with the presence of soluble high-molecular -weight α-syn species.

In conclusion, we report here a unique transgenic model of PD that exhibits early-onset circuit-specific deficits in dopamine neurotransmission followed subsequently by alterations in neuronal firing properties, a motor phenotype and neuron loss in the absence of overt protein aggregation pathology in the SNc and striatum. We therefore propose that PD-related phenotypes are not driven by progressive protein aggregation, but are associated with much earlier deficits in dopamine neurotransmission. Moreover, movement deficits might emerge when, on a foundation of sustained neurotransmission defects, some dopamine neurons die whereas those remaining decrease their firing. The *SNCA*-OVX mice allow us to advance our understanding of the cellular basis of changes to dopamine and non-dopamine neurotransmission in brain regions that differ in disease susceptibility and provide a model to test next-generation therapies.

Materials and Methods

Generation of Transgenic Mice. Transgenic mouse lines were generated by injection of BAC DNA containing the human wild-type *SNCA* locus into C57/Bl6 mouse pronuclei (Charles River). Transgene integrity and expression levels were analyzed (*SI Materials and Methods*) and two lines were chosen and back-crossed onto an α-syn-null (*Snca*$^{-/-}$) pure C57/Bl6 background (11) for nine generations to establish two transgenic lines, *SNCA*-OVX and hα-syn. The *SNCA* transgene was maintained in a hemizygous state on a pure

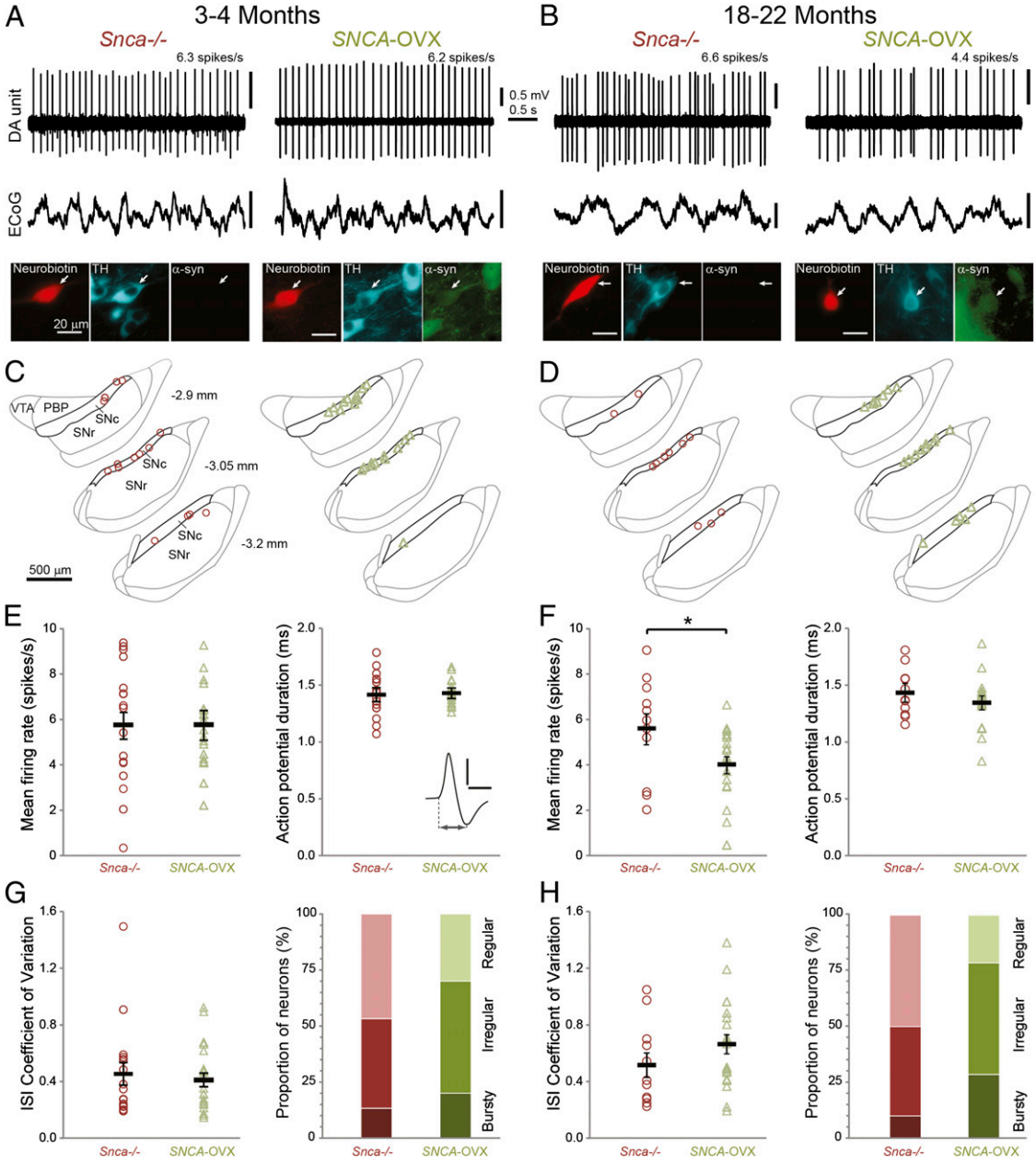

Fig. 6. Spontaneous firing of identified dopaminergic neurons in the substantia nigra in vivo. Unit activity of individual dopamine neurons recorded in (*A*) 3- to 4-mo-old and (*B*) 18- to 22-mo-old *Snca*$^{-/-}$ and *SNCA*-OVX mice during robust slow-wave activity in electrocorticograms (ECoG). Neurons were juxtacellularly labeled with Neurobiotin, verified as dopaminergic by TH expression, and tested for expression of α-syn. (*C* and *D*) Locations of identified dopamine neurons in (*C*) 3- to 4-mo-old and (*D*) 18- to 22-mo-old *Snca*$^{-/-}$ (red) and *SNCA*-OVX (green) mice (dorsal top, lateral right) grouped at three rostro-caudal levels (distances from bregma shown left). PBP, parabrachial pigmented nucleus of the VTA; SNc, substantia nigra pars compacta; SNr, substantia nigra pars reticulata; VTA, ventral tegmental area. [Adapted from ref. 23.] (*E* and *F*) Mean firing rates and action potential durations of SNc dopamine neurons in (*E*) 3- to 4-mo-old (n = 17, *Snca*$^{-/-}$ and 22 neurons, *SNCA*-OVX) and (*F*) 18- to 22-mo-old mice (n = 11 and 21; *$P < 0.05$). (*Inset*) Average wideband-filtered action potential from an *SNCA*-OVX mouse indicating duration measurement (scale 0.5 mV, 1 ms). (*G* and *H*) Mean interspike interval (ISI) coefficients of variation and the proportions of SNc neurons exhibiting each firing mode in (*G*) 3- to 4-mo-old mice (n = 15 and 20 neurons analyzed for mode in *Snca*$^{-/-}$ and *SNCA*-OVX) and (*H*) 18- to 22-mo-old mice (n = 10 and 14 neurons). The firing pattern did not differ significantly with genotype. In *E*–*H*, group means ± SEM are shown in black.

C57/Bl6 background. All procedures were conducted in accordance with the United Kingdom Animals (Scientific Procedures) Act of 1986 and approved by the local ethical review panel at the Department of Physiology, Anatomy and Genetics, University of Oxford.

Immunostaining. Animals were transcardially perfused with PBS (pH 7.4) followed by 4% paraformaldehyde (PFA) (vol/vol). Brains were postfixed in 4% PFA (vol/vol), cryoprotected in 30% sucrose, and sectioned on a freezing microtome (Leica Microsystems). For immunofluorescence, sections (35 μm) were incubated overnight with primary antibodies against α-syn (1:500; Covance) and TH (1:500; Millipore) and then incubated with goat anti-mouse Alexa 488 and goat anti-rabbit Alexa 594 antibody. For peroxidase immunohistochemistry, sections (50 μm) were incubated with primary antibodies against α-syn (1:1,000; BD Bioscience) or TH (1:2,000; Millipore). Sections were incubated with biotinylated secondary antibody followed by incubation in avidin–biotin–peroxidase complex and staining was visualized using 3,3′-diaminobenzidine (DAB). Sections were counterstained with hematoxylin, dehydrated, and coverslipped using DPX Mountant (Fluka Biochemika).

Western analysis. Striatal tissue was homogenized in phosphate buffered saline (pH 7.4) containing 1% (vol/vol) Igepal CA-630, 0.1% (vol/vol) SDS, 0.5% (mass/vol) sodium deoxycholate and protease inhibitor cocktail, using a Tissue Tearor (Biospec Products, Inc). Protein content was quantified using a BAC assay kit (Sigma) and proteins were analyzed by Western blotting. See Table S2 for primary antibodies. Bands were visualized using horseradish peroxidase-conjugated goat anti-mouse IgG (Bio-Rad) and the chemiluminescent ECL+ kit (GE Healthcare). Bands were quantified using ImageJ software. Data was analyzed using one-way ANOVA and Bonferroni post hoc analysis using SPSS Statistics 20 (IBM).

Neuropathology. To detect potential α-syn–related pathology, the mAbs Syn-1 (1:1,000; BD Transduction Labs) against aa 91–99 and LB509 (1:1,000; Invitrogen) against aa115–122 were used. Brains were fixed in 10% formalin (vol/vol), embedded in paraffin, and cut into 6-μm-thick sections, deparaffinized, and rehydrated. Peroxidase activity was eliminated by treatment with 3% H_2O_2 (mass/vol). Antigen retrieval for Syn-1 involved treatment with formic acid for 15 min, and for LB509 involved either autoclaving (121 °C) for 10 min in citrate buffer or treatment with 20 μg/mL proteinase K (Roche) for 10 min at room temperature. The mouse-on-mouse kit (M.O.M.; Vector Labs) was used to mAb to minimize the background and staining was visualized using DAB (Vector Labs). Thioflavine S staining was carried out as described by Sun et al. (22).

Stereological Cell Count. The total number of TH-immunoreactive and hematoxylin-counterstained nigral dopamine neurons was estimated with the optical fractionator method of unbiased stereology using the Stereo-Investigator software (MicroBrightField). Sections (50 μm) were processed for TH immunoreactivity as described above. Cells were counted under a 40× objective of a Zeiss Imager M2 microscope using a randomly placed counting frame of 50 × 50 μm on a sample grid of 120 × 160 μm. A 22-μm optical dissector with 2-μm upper and lower guard zones was used. The SNc was delineated using a mouse brain atlas (23). Every second section from 2.7 to 3.88 mm posterior to bregma was counted. Data are expressed as mean number of TH-immunoreactive neurons ± SEM and were analyzed using one-way ANOVA and Bonferroni post hoc analysis using SPSS Statistics 20 (IBM).

Behavior. ***One-hour stool collection.*** Animals (male and female) were placed into separate clean cages and fecal pellets were collected over a 1-h period (1600–1700 hours). Pellets were weighed to obtain wet stool weight, dried overnight at 65 °C, and reweighed to obtain dry stool weight and stool water content (24).

Rotarod. In the rotarod test, female mice were placed on a rod that accelerated from 4 to 40 rpm over a 5-min period. The length of time which the animals were able to stay on the rotating rod was recorded as latency to fall. Animals were tested three times a day for two consecutive days and performance was averaged for each day (20).

Multiple static rods test. In the multiple static rods test, two wooden dowels of 22-mm (rod 1) or 9-mm (rod 2) diameter were clamped to a supporting platform 50 cm above a cushioned surface. Female mice were placed at the end of the rod facing away from the platform. The time taken to turn around by 180° to face the platform, time taken to traverse the rod, and the number of foot slips made when traversing the rod were recorded (20).

Forepaw stride length. In the forepaw stride length test, animals' forepaws were placed in ink and animals walked across a sheet of paper toward their home cage. The distance between steps on the same side of the body, from the middle toe of the first step to the heel of the second step, was measured and averaged to obtain stride length. Only steps during normal walking (straight line, no stopping) were included in the analysis (24). Male and female animals were tested.

Statistics. Data analyzed using a parametric one-, two- or three-way ANOVA followed by a Tukey post hoc test are expressed as means ± SEM. Data analyzed using a nonparametric Kruskal–Wallis ANOVA followed by Dunn's pairwise multiple comparison are expressed as median ± interquartile (IQ) range. Analyses were completed using the SPSS Statistics 21 software (IBM).

FCV. Mice were killed by cervical dislocation and decapitated. Coronal slices (300 μm) containing the region of interest (striatum, BNST, or SNr) were prepared as described previously (15, 25) in ice-cold Hepes-buffered artificial cerebrospinal fluid (aCSF) saturated with 95% O_2/5% CO_2. Slices were then maintained in a bicarbonate-buffered aCSF at room temperature before recording. Extracellular dopamine, NE, or 5-HT concentration ($[dopamine]_o$, $[NE]_o$, or $[5\text{-}HT]_o$) were monitored using FCV with 7-μm-diameter carbon fiber microelectrodes (tip length 50–100 μm) and a Millar Voltammeter (Julian Millar, Barts and the London School of Medicine and Dentistry, London, UK) as described previously (15, 26, 27). In brief, the scanning voltage was a triangular waveform (–0.7 V to +1.3 V range vs. Ag/AgCl) at a scan rate of 800 V/s and frequency of 8 Hz. Electrodes were calibrated in 0.5–2 μM 5-HT, dopamine, or NE in experimental media. All data are expressed as means ± SEM, and the sample size, *n*, is the number of observations. The number of animals in each FCV dataset was ≥3. Comparisons for differences in means were assessed by two-way ANOVA and post hoc Bonferroni *t* test or unpaired *t* test using GraphPad Prism 4.0 (GraphPad Software).

HPLC with Electrochemical Detection. Dopamine content was measured by HPLC with electrochemical detection as described previously (16, 20). Following FCV recordings, tissue punches from the dorsal (2 mm in diameter) and ventral striatum (1.2 mm in diameter) from two brain slices per animal were taken and analyzed for dopamine content by HPLC.

Electron Microscopy. Ultrastructural analyses were performed on 3-mo-old mice. Three *SNCA-OVX* and three littermate $Snca^{-/-}$ animals were anesthetized and perfuse-fixed with 0.1% glutaraldehyde and 4% PFA (vol/vol) in 0.1 M phosphate buffer. Sagittal vibratome sections (60 μm) were incubated with primary antibody against TH to identify dopamine neurons, followed by a gold-conjugated secondary antibody and silver-intensification of the gold particles (see ref. 28). Sections were subsequently postfixed in 1% osmium tetroxide and mounted on slides in an electron microscopic resin. Samples of dorsolateral striatum were identified, cut from the sections, and reembedded onto resin blocks and serial ultrathin sections (50–70 nm) were collected and stained with lead citrate. For each animal, 50 images of TH-immunoreactive structures were acquired in a systematically randomized manner (150 images per genotype). In addition, TH-immunoreactive structures forming synaptic specializations were randomly acquired (*SNCA-OVX* = 33; $Snca^{-/-}$ = 29). Digital images of TH-immunoreactive structures and synapses were analyzed using ImageJ and ImageJ plugins PointDensity and PointDensitySyn (16, 29) to measure terminal size, length of synaptic active zone, vesicle number, and distribution. At all stages of tissue processing and ultrastructural analysis the investigators were blinded to animal genotype. Statistical tests were performed using SPSS/PASW Statistics (SPSS) and Matlab (Mathworks).

In Vivo Electrophysiological Recording and Juxtacellular Labeling of Single Neurons. Experiments were performed in urethane-anesthetized (1.5 g/kg, i.p.) 3- to 4-mo-old mice (five $Snca^{-/-}$ and six *SNCA*-OVX) and 18- to 22-mo-old mice (five $Snca^{-/-}$ and six *SNCA*-OVX). Extracellular recordings of single-unit activity in the SNc were made using glass electrodes (10–25 MΩ in situ; tip diameter ~1.5 μm) containing 0.5 M NaCl solution and Neurobiotin (1.5% wt/vol; Vector Laboratories). An electrocorticogram was also recorded above the frontal cortex (18). Following electrophysiological characterization, single neurons were juxtacellularly labeled with Neurobiotin for post hoc verification of location and neurochemical identity (18). We focused our analysis on single-unit activity recorded during robust slow-wave activity, as quantitatively defined from the simultaneous electrocorticogram recordings. Firing pattern was defined according to one of three modes (regular, bursty, or irregular), as detailed previously (30, 31) and in *SI Materials and Methods*. Before statistical comparisons, a Shapiro–Wilk test was used to judge whether datasets were normally distributed ($P < 0.05$ to reject). Statistical comparisons were made using Student *t* tests or Welch *t* tests. The prevalence of firing patterns was compared with a Fisher's exact test.

ACKNOWLEDGMENTS. We thank J. Alegre-Abarrategui, R. Deacon, K. Jennings, C. Johnson, and E. Pissadaki for their expertise in experimental techniques. We thank E. Volpi (Cytogenetics Core, Wellcome Trust Centre for Human Genetics, Oxford; Wellcome Trust Core Award, Grant 090532/Z/09/Z) for FISH analysis. We thank the animal care and veterinary support staff at Oxford University Biomedical Services. This work was supported by the Monument Trust Discovery Award from Parkinson's UK, Wellcome Trust Research Career Development Fellowship GR073141MA (to R.W.-M.), Medical Research Council (MRC) UK Awards U138164490 and U138197109 (to J.P.B. and P.J.M., respectively), and Wellcome Trust Neuroscience Studentship in Neuroscience GR072324MA (to S.L.S.). M.J.D. holds a Girdlers' New Zealand Health Research Council Fellowship; S.J., D.P., and S.A. hold MRC studentships; P.K. is supported by the Clarendon Fund; and D.M.B. holds a Wellcome Trust Senior Research Fellowship.

1. Chesselet M-F, Richter F (2011) Modelling of Parkinson's disease in mice. *Lancet Neurol* 10(12):1108–1118.
2. Polymeropoulos MH, et al. (1997) Mutation in the alpha-synuclein gene identified in families with Parkinson's disease. *Science* 276(5321):2045–2047.
3. Krüger R, et al. (1998) Ala30Pro mutation in the gene encoding alpha-synuclein in Parkinson's disease. *Nat Genet* 18(2):106–108.
4. Zarranz JJ, et al. (2004) The new mutation, E46K, of alpha-synuclein causes Parkinson and Lewy body dementia. *Ann Neurol* 55(2):164–173.
5. Chartier-Harlin MC, et al. (2004) Alpha-synuclein locus duplication as a cause of familial Parkinson's disease. *Lancet* 364(9440):1167–1169.
6. Singleton AB, et al. (2003) alpha-Synuclein locus triplication causes Parkinson's disease. *Science* 302(5646):841.
7. Satake W, et al. (2009) Genome-wide association study identifies common variants at four loci as genetic risk factors for Parkinson's disease. *Nat Genet* 41(12):1303–1307.
8. Simón-Sánchez J, et al. (2009) Genome-wide association study reveals genetic risk underlying Parkinson's disease. *Nat Genet* 41(12):1308–1312.
9. Venda LL, Cragg SJ, Buchman VL, Wade-Martins R (2010) α-Synuclein and dopamine at the crossroads of Parkinson's disease. *Trends Neurosci* 33(12):559–568.
10. Miller DW, et al. (2004) Alpha-synuclein in blood and brain from familial Parkinson disease with SNCA locus triplication. *Neurology* 62(10):1835–1838.
11. Abeliovich A, et al. (2000) Mice lacking alpha-synuclein display functional deficits in the nigrostriatal dopamine system. *Neuron* 25(1):239–252.
12. Neumann M, et al. (2002) Misfolded proteinase K-resistant hyperphosphorylated alpha-synuclein in aged transgenic mice with locomotor deterioration and in human alpha-synucleinopathies. *J Clin Invest* 110(10):1429–1439.
13. Robertson DC, et al. (2004) Developmental loss and resistance to MPTP toxicity of dopaminergic neurones in substantia nigra pars compacta of gamma-synuclein, alpha-synuclein and double alpha/gamma-synuclein null mutant mice. *J Neurochem* 89(5):1126–1136.
14. Al-Wandi A, et al. (2010) Absence of alpha-synuclein affects dopamine metabolism and synaptic markers in the striatum of aging mice. *Neurobiol Aging* 31(5):796–804.
15. Threlfell S, et al. (2012) Striatal dopamine release is triggered by synchronized activity in cholinergic interneurons. *Neuron* 75(1):58–64.
16. Anwar S, et al. (2011) Functional alterations to the nigrostriatal system in mice lacking all three members of the synuclein family. *J Neurosci* 31(20):7264–7274.
17. Nemani VM, et al. (2010) Increased expression of alpha-synuclein reduces neurotransmitter release by inhibiting synaptic vesicle reclustering after endocytosis. *Neuron* 65(1):66–79.
18. Brown MT, Henny P, Bolam JP, Magill PJ (2009) Activity of neurochemically heterogeneous dopaminergic neurons in the substantia nigra during spontaneous and driven changes in brain state. *J Neurosci* 29(9):2915–2925.
19. Gründemann J, Schlaudraff F, Haeckel O, Liss B (2008) Elevated alpha-synuclein mRNA levels in individual UV-laser-microdissected dopaminergic substantia nigra neurons in idiopathic Parkinson's disease. *Nucleic Acids Res* 36(7):e38.
20. Senior SL, et al. (2008) Increased striatal dopamine release and hyperdopaminergic-like behaviour in mice lacking both alpha-synuclein and gamma-synuclein. *Eur J Neurosci* 27(4):947–957.
21. Smith Y, Kieval JZ (2000) Anatomy of the dopamine system in the basal ganglia. *Trends Neurosci* 23(10, Suppl):S28–S33.
22. Sun A, Nguyen XV, Bing G (2002) Comparative analysis of an improved thioflavin-s stain, Gallyas silver stain, and immunohistochemistry for neurofibrillary tangle demonstration on the same sections. *J Histochem Cytochem* 50(4):463–472.
23. Franklin KBJ, Paxinos G (2007) *The Mouse Brain in Stereotaxic Coordinates* (Academic, New York), 3rd Ed.
24. Taylor TN, et al. (2009) Nonmotor symptoms of Parkinson's disease revealed in an animal model with reduced monoamine storage capacity. *J Neurosci* 29(25):8103–8113.
25. Threlfell S, et al. (2010) Striatal muscarinic receptors promote activity dependence of dopamine transmission via distinct receptor subtypes on cholinergic interneurons in ventral versus dorsal striatum. *J Neurosci* 30(9):3398–3408.
26. Jennings KA, Lesch KP, Sharp T, Cragg SJ (2010) Non-linear relationship between 5-HT transporter gene expression and frequency sensitivity of 5-HT signals. *J Neurochem* 115(4):965–973.
27. Threlfell S, et al. (2004) Histamine H3 receptors inhibit serotonin release in substantia nigra pars reticulata. *J Neurosci* 24(40):8704–8710.
28. Moss J, Bolam JP (2008) A dopaminergic axon lattice in the striatum and its relationship with cortical and thalamic terminals. *J Neurosci* 28(44):11221–11230.
29. Larsson M, Broman J (2005) Different basal levels of CaMKII phosphorylated at Thr286/287 at nociceptive and low-threshold primary afferent synapses. *Eur J Neurosci* 21(9):2445–2458.
30. Tepper JM, Martin LP, Anderson DR (1995) GABAA receptor-mediated inhibition of rat substantia nigra dopaminergic neurons by pars reticulata projection neurons. *J Neurosci* 15(4):3092–3103.
31. Paladini CA, Tepper JM (1999) GABA(A) and GABA(B) antagonists differentially affect the firing pattern of substantia nigra dopaminergic neurons in vivo. *Synapse* 32(3):165–176.

Supporting Information

Janezic et al. 10.1073/pnas.1309143110

SI Materials and Methods

Experimental Animals. For behavioral analysis, equal numbers of male and female mice were used. Where a sex-dependent change was found, this is indicated in the results. If no difference was found between genders, data were pooled. For molecular analysis, including immunohistochemistry, Western blotting analysis, pathology, stereological cell counting, and immunoprecipitation analysis, both male and female animals were analyzed. For fast-scan cyclic voltammetry (FCV) recordings, sex-matched pairs of human wild-type alpha-synuclein overexpression (*SNCA*-OVX) and alpha-synuclein knockout ($Snca^{-/-}$) or human wild-type physiological expressor (hα-syn) and ($Snca^{-/-}$) mice were used for recordings. Electrophysiological recordings were taken from male mice.

FISH. Primary fibroblasts were extracted for FISH analysis using a protocol adapted from Kulnane et al. (1). Confluent cells were used for the generation of metaphase spreads and FISH analysis was performed using bacterial artificial chromosome (BAC) DNA as probe.

Western Analysis. Protein extraction and Western analysis was performed as previously described (2, 3). Striatal tissue was homogenized in PBS (pH 7.4) containing 1% Igepal CA-630, 0.1% SDS, 0.5% sodium deoxycholate, and protease inhibitor mixture using a Tissue Tearor (Biospec Products, Inc.) or sonicated for 10 s in 1% (wt/vol) SDS. Protein content was quantified using a BCA assay kit (Sigma) and proteins were analyzed by Western blotting. Primary antibodies used are described in Table S2. Bands were visualized using horseradish peroxidase-conjugated goat anti-mouse, goat anti-rabbit, goat anti-guinea pig, or goat anti-rat IgG (Bio-Rad) and the chemiluminescent ECL^{+} kit (GE Healthcare). Bands were quantified using ImageJ software (4). Data were analyzed using one-way ANOVA and Bonferroni post hoc analysis using SPSS Statistics 20 (IBM).

Analysis of Posttranslational α-syn Modifications. Posttranslationally modified α-syn species were isolated from the midbrain from 3- and 18-mo-old mice, or Parkinson disease (PD) nigral tissue, as previously described (5). Briefly, samples were lysed into non-detergent lysis buffer [50 mm Tris·HCl (pH 7.4), 175 mm NaCl, and 5 mm EDTA (pH 8.0) with protease inhibitor and phosphatase inhibitor mixture] by sonication for 10 s. Samples were incubated in Triton X-100 for 30 min on ice then centrifuged at 15,000 × *g* for 60 min at 4 °C. The supernatant (Triton-soluble fraction) was removed and used for analysis of posttranslational modifications. For the analysis of α-syn high-molecular-weight species, samples (25 μg) were subjected to native PAGE at 85 V for 4.5 h and equal protein loading was confirmed by Ponceau S staining. Blots were probed using a rabbit monoclonal anti–α-syn antibody (clone MJFR1; Abcam). For the analysis of α-syn truncations or S129 phosphorylation samples (10 μg) were subjected to reducing, denaturing SDS/PAGE and probed for truncation using mouse monoclonal anti–α-syn antibody, raised against aa 15–123 of α-syn (clone 42; BD biosciences). Blots were subsequently stripped and reprobed using the C-terminal (aa 118–123) MJFR1 antibody. For analysis of S129 phosphorylation, lysates were used both pre- and post-Triton extraction. Blots were probed using either a mouse monoclonal (clone 64; WAKO), a rabbit monoclonal (EP1536Y; Abcam), or a rabbit polyclonal anti-phospho S129 α-synuclein antibody (ab59264; Abcam). Blots were reprobed using both β-actin and MJFR1 α-synuclein antibodies to confirm loading.

Neuropathology. To detect potential α-syn–related pathology, the mAbs Syn-1 (1:1,000; BD Transduction Labs) against aa 91–99 and LB509 (1:1,000; Invitrogen) against aa 115–122 were used. Other antibodies included anti-p62, ubiquitin binding protein/sequestosome 1 (1:5,000; Enzo); anti-GFAP (1:4,000; Dako); anti–Iba-1 (1:2,000; WAKO); anti-AT8, phospho-tau recognizing phosphorylated serine 202/threonin 205 (1:500; Innogenetics); and anti-4G8, β-amyloid (1:5,000;Covance). Brains were fixed in 10% formalin, embedded in paraffin, and cut into 6-μm-thick sections, deparaffinized, and rehydrated. Peroxidase activity was eliminated with treatment with 3% H_2O_2 followed by pretreatments with either formic acid for 15 min (Syn-1, 4G8), autoclaving (121 °C) for 10 min in citrate buffer (LB509, p62, Iba-1), 20 μL/mL proteinase K (Roche) treatment for 10 min (LB509), or microwaving in citrate buffer three times for 5 min (GFAP). The mouse-on-mouse kit (M.O.M.; Vector Labs) was used to mAb to minimize the background and staining was visualized using 3,3′-diaminobenzidine (Vector Labs).

Behavior. ***One-hour stool collection.*** Animals were placed into separate clean cages and fecal pellets were collected over a 1-h period (1600–1700 hours). Pellets were weighed to obtain wet stool weight, dried overnight at 65 °C, and reweighed to obtain dry stool weight and stool water content (6).

Inverted screen. The inverted screen test was performed as described previously (7). The mouse was placed into the center of a 50- × 50-cm^2 wire grid framed by a 4-cm wooden frame, with a mesh of 12-mm squares of 1 mm in diameter. The grid was then immediately inverted with the head of the mouse declining first and held 50 cm above a soft surface. The latency to fall was recorded for each mouse, with a maximum trial time of 60 s.

FCV. Mice of mixed sex 3 to 18 mo old were killed by cervical dislocation and decapitated, and their brains were removed over ice. Coronal slices (300 μm) were cut using a vibratome (VT 1200S; Leica) in ice-cold Hepes-buffered artificial cerebrospinal fluid (aCSF) containing 120 mM NaCl, 5 mM KCl, 20 mM $NaHCO_3$, 6.7 mM Hepes acid, 3.3 mM Hepes salt, 2 mM $CaCl_2$, 2 mM $MgSO_4$, 1.2 mM KH_2PO_4, and 10 mM glucose and saturated with 95% O_2/5% CO_2. After a minimum of 1 h of recovery at room temperature slices were then transferred to the recording chamber and maintained in an oxygenated bicarbonate-buffered aCSF containing 124 mM NaCl, 3.7 mM KCl, 26 mM $NaHCO_3$, 2.4 mM $CaCl_2$, 1.3 mM $MgSO_4$, 1.3 mM KH_2PO_4, and 10 mM glucose as described previously (2, 8, 9). Superfusion flow rate was ∼1.5 mL/min. Extracellular concentration of electrically evoked amines were monitored and quantified at 32 °C using FCV with 7-μm-diameter carbon-fiber microelectrodes (exposed tip length 50–100 μm, fabricated in-house) and a Millar voltammeter (Julian Millar, Barts and The London School of Medicine and Dentistry, London, UK). The applied voltage was a triangular waveform, with a voltage range of −0.7 to 1.3 to −0.7 V vs. Ag/AgCl at a scan rate of 800 V/s, with a sampling frequency of 8 Hz. Electrodes were positioned in brain slices to a depth of 100 μm. Amine release was evoked locally by a surface, concentric bipolar Pt/Ir electrode (25-μm diameter; FHC) placed ∼150 μm away from the carbon-fiber microelectrode as described previously (2, 8, 9). Stimulus pulses were generated out-of-phase with FCV scans and were applied at the lowest

current that generated maximal dopamine release with a single stimulus pulse in wild-type animals (600–650 μA, 200-μs pulse duration).

Detection of Dopamine Release in Striatum. Extracellular dopamine concentration ($[dopamine]_o$) was monitored and quantified in dorsal and ventral striatum. The evoked current signal was confirmed as dopamine by comparing the peak potentials for oxidation and reduction currents with those of dopamine in calibration media (+500–600 and −200 mV vs. Ag/AgCl, respectively). Electrodes were calibrated in 1–2 μM dopamine following experiments in all experimental media. FCV experiments assessed $[dopamine]_o$ evoked by discrete stimuli in the caudate-putamen (CPu) and nucleus accumbens (NAc). Recording sites classed as CPu were located dorsal to the anterior commissure; NAc was ventral and medial of anterior commissure (Fig. 3*G*). Data were collected through one of two experimental designs. First, several sites were sampled per slice (six CPu and two NAc) in both genotypes from two slices on the same experimental day. Stimuli in these experiments consisted of either a single pulse or four pulses at 100 Hz separated by 2.5 min, and alternating between genotypes (either *SNCA*-OVX or hα-syn and *Snca*$^{-/-}$). The two genotypes being compared on a given recording day would be age- and sex-matched (e.g., male *SNCA*-OVX and male *Snca*$^{-/-}$). In the second stimulation paradigm, in particular when investigating mechanisms underlying the dopamine release deficit in CPu, recordings were taken at a single recording site at 2.5-min intervals to ensure consistent release and consisted of either single pulses or trains of four pulses at a range of frequencies (1–100 Hz) in randomized order. These frequencies span the full range of dopaminergic neuron firing frequencies reported in vivo. For these experiments in CPu, recording sites were made in the dorsal half of the CPu close to the corpus callosum, and recordings from only one genotype per day were made. Animals used in these mechanistic experiments were between 3 and 8 mo old.

HPLC with Electrochemical Detection. Dopamine content in dorsal and ventral striatum was measured by HPLC with electrochemical detection as described previously (2, 10). Following FCV recordings, tissue punches from the dorsal (2 mm in diameter) and ventral striatum (1.2 mm in diameter) from two brain slices per animal were taken and stored at −80 °C in 200 μL 0.1 M $HClO_4$. On the day of analysis, samples were thawed, homogenized, and centrifuged at 16,000 × *g* for 15 min at 4 °C. The supernatant was analyzed for dopamine content using HPLC with electrochemical detection. Analytes were separated using a 4.6- × 250-mm Microsorb C18 reverse-phase column (Varian or Agilent) and detected using a Decade II SDS electrochemical detector with a Glassy carbon working electrode (Antec Leyden) set at + 0.7 V with respect to a Ag/AgCl reference electrode. The mobile phase consisted of 13% methanol (vol/vol), 0.12 M NaH_2PO_4, 0.5–4.0 mM octenyl succinic anhydride (OSA), and 0.8 mM EDTA (pH 3.1–4.6), and the flow rate was fixed at 1 mL/min. Analyte measurements were normalized to tissue-punch volume.

Drugs. Dihydro-β-erythroidine (DHβE) and cocaine were purchased from Tocris Bioscience or Sigma-Aldrich, and all other reagents were purchased from Sigma-Aldrich, Fisher Scientific, or VWR. Drugs were dissolved in distilled water to make stock aliquots at 1,000–10,000 × final concentrations and stored at −20 °C until required. Stock aliquots were diluted with oxygenated aCSF to the final concentration immediately before use.

Immunoprecipitations. Striatal brain tissue was homogenized in 50 mM Tris (pH 7.5) with 150 mM NaCl, 1% Triton X-100, and protease inhibitor. Brain lysates were incubated for 2 h at 4 °C with 50 μL of a 50% slurry of protein-G Sepharose beads (GE Healthcare), which were preincubated with mouse anti-SNAP25 primary antibody (BD Bioscience) for 2 h at room temperature. Beads were subjected to four washes with lysis buffer and proteins were eluted with 2× Laemilli buffer and boiled at 95 °C for 10 min. Coprecipitated proteins were analyzed using SDS/PAGE and normalized to the amount of precipitated SNAP25 protein. Control precipitations were carried out using beads without preincubation with antibody.

Detection of Norepinephrine Release in Bed Nucleus of the Stria Terminalis. Norepinephrine (NE) release was monitored and quantified in the ventromedial portion of the bed nucleus of the stria terminalis (vmBNST). Catecholamine detection using FCV has previously been described in vmBNST (11), although the distinction between dopamine and NE had not been previously made. NE and dopamine have similar oxidation and reduction peak potentials. Evoked signals were readily attributable to catecholamines by comparison of potentials for peak oxidation and reduction currents with those of NE or dopamine in calibration media (+500–600 mV and −200 mV vs. Ag/AgCl, respectively). However, we attributed signals recorded in vmBNST to NE rather than dopamine, by confirming that these signals were regulated by the α2-adrenergic receptor antagonist idazoxan and the NE transporter inhibitor despiramine, which did not, in contrast, modify dopamine signals in the CPu. Electrode calibrations were completed in the recording chamber postexperiment with 2 μM NE in aCSF at 32 °C. Unless otherwise stated, individual data points were obtained from recordings taken repeatedly at a single recording site at 7-min intervals, to ensure consistent release (11), and consisted of trains of 30 pulses at a range of frequencies (10–100 Hz) in randomized order.

Detection of 5-Hydroxytryptamine Release in Substantia Nigra Pars Reticulata. 5-Hydroxytryptamine (5-HT) release was monitored and quantified in the substantia nigra pars reticulata (SNr) as described previously (12, 13). Individual data points were obtained from recordings taken from three discrete recording sites in the ventral portion of the SNr (~3.0–3.5 mm posterior to bregma) close to the cerebral peduncle to minimize the likelihood of somatodendritic dopamine contributing to recorded signals (Fig. 5*B*). Evoked signals were readily attributable to the indoleamine, 5-HT, by comparison of potentials for peak oxidation and dual reduction currents with those of 5-HT in calibration media (+550 mV and −20 and −400 mV vs. Ag/AgCl, respectively). Signals containing mixed reduction profiles that were not readily attributable to 5-HT were not included in the analysis. Electrode calibrations were completed in the recording chamber postexperiment with 0.5 μM 5-HT in aCSF at 32 °C.

Electrophysiological Recordings in Vivo. Experimental procedures were performed on 3- to 4-mo-old mice (five *Snca*$^{-/-}$, median age 103 d and six *SNCA-OVX*, median age 118 d) and 18- to 22-mo-old mice (five SNCA $^{-/-}$, median age 628 d and six SNCA OVX, median age 625 d) and were conducted in accordance with the Animals (Scientific Procedures) Act of 1986 (United Kingdom). Experiments and analyses were performed blind to genotype. Anesthesia was induced with 2% isoflurane (Isoflo; Schering-Plough) and maintained with urethane (1.5 g/kg, i.p.) (ethyl carbamate; Sigma). Supplemental doses of urethane (0.15 g/kg, i.p.) were given as required; anesthesia levels were assessed by examination of the electrocorticogram (ECoG; discussed below), ECG, and respiration rate/depth and by testing reflexes to a cutaneous pinch or gentle corneal stimulation. All wound margins were infiltrated with the local anesthetic bupivacaine (0.75% wt/vol; Astra) and corneal dehydration was prevented with application of Hypromellose eye drops (Norton Pharmaceuticals). Electrophysiology protocols were similar to those detailed for recordings of identified dopaminergic neurons in rats (14). Briefly, animals were placed in a stereotaxic frame (Kopf) and

body temperature was maintained at 37 ± 0.5 °C using a homeothermic heating device (Harvard Apparatus). The ECoG was recorded via a 0.8-mm-diameter steel screw juxtaposed to the dura mater above the right frontal cortex (anteroposterior 2 mm, mediolateral 1.5 mm in relation to bregma) (15) and was referenced against another screw implanted in the skull above the cerebellum. Raw ECoG was filtered (0.3–1,500 Hz, −3-dB limits) and amplified (2,000 times, DPA-2FS filter/amplifier; Scientifica) before acquisition. A discrete craniotomy was performed above the right and/or left substantia nigra (SN) and saline solution (0.9% wt/vol NaCl) was applied to exposed cortex to prevent dehydration. Extracellular recordings of the action potentials ("spikes") of single neurons (i.e., single-unit activity) were made using glass electrodes (GC120F-10; Harvard Apparatus; tip diameter ∼1.5 mm; 10–25 MW in situ), that contained saline solution (0.5 M NaCl) and Neurobiotin (1.5% wt/vol; Vector Laboratories). Electrode signals were amplified (10 times) through the active bridge circuitry of an Axoprobe-1A amplifier (Molecular Devices Corp.), bifurcated, then filtered differently to extract local field potentials (LFPs) or unit activity. The LFPs were recorded after further amplification (100 times; DPA-2FS) and "wideband" filtering (between 0.3 and 5,000 Hz; DPA-2FS). Unit activity was recorded after alternating current coupling, further amplification (100 times; DPA-2FS), and "standard bandpass" filtering (between 300 and 5,000 Hz; DPA-2FS). A Humbug (Quest Scientific) was used in place of a traditional "notch" filter to eliminate mains noise at 50 Hz. Spikes were often several millivolts in amplitude and always exhibited an initial positive deflection. We used generous on-line criteria (spike duration for standard bandpass-filtered spikes of >0.7 ms and firing rate of <15 Hz) to guide our recordings of putative dopaminergic SN neurons. These criteria not only cover more than the full scope of dopaminergic neuron firing in vivo (thus, minimizing recording bias), but also, by design, allowed us to avoid unnecessary recording of nondopaminergic neurons in the SNr and structures overlaying the SN (14, 16).

Juxtacellular Labeling of Single Neurons. To unambiguously locate recorded neurons and enable an analysis of their neurochemical properties, single units were labeled with Neurobiotin by the juxtacellular method (14). Briefly, the electrode was advanced slowly toward the neuron while a microiontophoretic current was applied (1–10 nA positive current, 200-ms duration, 50% duty cycle). The optimal position of the electrode was identified when the firing pattern of the neuron was robustly modulated by the current injection. The Neurobiotin was then left to transport along neuronal processes for up to 12 h. After the recording and labeling sessions, the animals were given a lethal dose of anesthetic and perfused via the ascending aorta with 20 mL of 0.01 M PBS at pH 7.4, followed by 20 mL of 4% (wt/vol) paraformaldehyde in 0.1 M phosphate buffer, pH 7.4. In some cases 0.1% glutaraldehyde was added to the paraformaldehyde; this was then followed by perfusion of 20 mL 4% (wt/vol) paraformaldehyde without glutaraldehyde. Brains were then left in fixative solution at 4 °C until they were sectioned 12–72 h later.

Tissue Processing for Identification of Recorded and Labeled Neurons. The fixed brains were sectioned at 50 μm in the coronal plane on a vibrating blade microtome (VT1000S; Leica Microsystems), collected in series, and washed in PBS. To locate Neurobiotin-labeled cells, free-floating tissue sections were then incubated for 4 h at room temperature in Triton PBS [PBS with 0.3% (vol/vol) Triton X-100 (Sigma)] containing Cy3-conjugated streptavidin (1:1,000 dilution; GE Healthcare). Sections containing Neurobiotin-labeled neuronal somata (those marked with Cy3) were then isolated for molecular characterization by indirect immunofluorescence. All identified SN neurons were tested for expression of tyrosine hydroxylase (TH) and α-synuclein. Briefly, sections were first incubated overnight at room temperature in Triton PBS containing the following primary antibodies: rabbit anti-TH (1:1,000, AB152; Millipore) and mouse anti- α-synuclein (1:500, 4B12; Covance). After washing in PBS, sections were incubated for 4 h at room temperature in PBS containing fluorophore-conjugated secondary antibodies to visualize immunoreactivity for TH (AMCA-conjugated donkey anti-rabbit IgG, 1:500; Jackson Immunoresearch Laboratories) and α-synuclein (Alexa Fluor 488-conjugated donkey anti-mouse IgG, 1:1,000; Invitrogen). Secondary antibodies were highly cross-adsorbed by the manufacturers to reduce cross-species reactivity. Sections were then washed in PBS and mounted on slides for viewing with a conventional epifluorescence microscope (Imager M2; Zeiss) equipped with a 40× 1.3 N.A. lens, a Prior Lumen200 fluorescent light source (Prior Scientific Inc.), and a Hamamatsu ORCA-ER monochrome digital camera (Hamamatsu Photonics K.K.). Images were acquired with Axiovision software (Carl Zeiss AG), using filters for Cy3 (excitation 532–558 nm, beamsplitter 570 nm, emission 570–640 nm), AMCA (excitation 365 nm SP, beamsplitter 395 nm, emission 420–470 nm), and Alexa Fluor 488 (excitation 450–490 nm, beamsplitter 495 nm, emission 500–550 nm). Absence of cross-talk between channels or "bleed through" was ensured for each fluorescence reaction. A neuron was classified as not expressing the tested molecular marker only when positive immunoreactivity could be observed in other cells on the same focal plane as the tested neuron. Digital images were cropped to regions of interest, with brightness and contrast adjusted when necessary, using Photoshop software (Adobe Systems). Only neurochemically identified dopaminergic neurons (i.e., those expressing TH immunoreactivity) located within the substantia nigra pars compacta (SNc) were included in our analyses.

Electrophysiological Data Analysis. All biopotentials were digitized online at 19.8 kHz with a Power 1401 analog–digital converter (Cambridge Electronic Design). Data were acquired and initially analyzed using Spike2 software (version 7.07; Cambridge Electronic Design). Because the firing pattern, but not firing rate, of SN dopaminergic neurons varies as a function of brain state (14), we focused our analysis on unit activity recorded during robust slow-wave activity (SWA), as verified by simultaneous ECoG recordings (Fig. 6*A*). To extract SWA periods in an objective way, ECoG data were Fourier-transformed (frequency resolution of 0.2 Hz), and the ratio of power in the SWA band (0.5–2 Hz) to power in the gamma band (30–80 Hz) was calculated. Epochs of contiguous data (each of >10 s in duration) where each data point had a power ratio of >13 were then concatenated and used for further analysis (mean duration of analyzed epochs 198.17 ± 11.55 s, $n = 69$). After identifying epochs, putative single-unit activity was isolated with standard "spike-sorting" procedures, including template matching, principal component analysis, and supervised clustering (Spike2). Isolation of single units was verified by the presence of a distinct refractory period in the interspike interval (ISI) histograms. Mean firing rate (spikes per second) was calculated from the total number of spikes per data epoch. The coefficient of variation of the ISI (CV), a value used widely as an indicator of regularity in point processes, was calculated (the lower the CV value, the more regular the unit activity). Measurements of the mean extracellularly recorded spike waveform were also taken from the wideband-filtered traces; after waveform interpolation (cubic spline function, Spike2) spike threshold was defined as 15% of the differential of the waveform upstroke, and spike duration was then measured from this threshold to the first trough (14). To further define firing pattern, autocorrelograms (2-ms bins, plotted over 1 s) were constructed from epochs containing more than 300 spikes. Firing pattern was classified according to one of three modes, using a method similar to that detailed previously (17, 18); briefly, dopaminergic neurons that

exhibited three or more equally spaced peaks in the autocorrelogram were classified as "regular," those that exhibited a distinct initial peak (at an interval shorter than the mean ISI) followed by a return to steady firing rate were classified as "bursty," and all other neurons were classified as "irregular." Autocorrelograms were independently examined by three investigators and firing pattern ascribed according to the modal classification.

Statistical Analysis. For behavior, data were analyzed using a parametric one-, two- or three-way ANOVA followed by a Tukey post hoc test and expressed as means ± SEM. Data analyzed using a nonparametric Kruskal–Wallis ANOVA followed by Dunn's pairwise multiple comparison are expressed as median ± interquartile (IQ) range. Analyses were completed using the SPSS Statistics 21 software (IBM). For FCV, all data are expressed as means ± SEM, and the sample size, n, is the number of observations. The number of animals in each data set was ≥3. Comparisons for differences in means were assessed by two-way ANOVA and post hoc Bonferroni t test or unpaired t test using GraphPad Prism 4.0 (GraphPad Software). For electrophysiology, before statistical comparisons a Shapiro–Wilk test was used to judge whether datasets were normally distributed ($P < 0.05$ to reject). Statistical comparisons were made using Student t tests except for datasets that were not normally distributed or had unequal variance, where Welch t tests were used. The prevalence of firing patterns was compared with a Fisher's exact test.

1. Kulnane LS, Lehman EJ, Hock BJ, Tsuchiya KD, Lamb BT (2002) Rapid and efficient detection of transgene homozygosity by FISH of mouse fibroblasts. *Mamm Genome* 13(4):223–226.
2. Anwar S, et al. (2011) Functional alterations to the nigrostriatal system in mice lacking all three members of the synuclein family. *J Neurosci* 31(20):7264–7274.
3. Caudle WM, et al. (2007) Reduced vesicular storage of dopamine causes progressive nigrostriatal neurodegeneration. *J Neurosci* 27(30):8138–8148.
4. Schneider CA, Rasband WS, Eliceiri KW (2012) NIH Image to ImageJ: 25 years of image analysis. *Nat Methods* 9(7):671–675.
5. Klucken J, Shin Y, Masliah E, Hyman BT, McLean PJ (2004) Hsp70 Reduces alpha-Synuclein Aggregation and Toxicity. *J Biol Chem* 279(24):25497–25502.
6. Taylor TN, et al. (2009) Nonmotor symptoms of Parkinson's disease revealed in an animal model with reduced monoamine storage capacity. *J Neurosci* 29(25): 8103–8113.
7. Contet C, Rawlins JN, Deacon RM (2001) A comparison of 129S2/SvHsd and C57BL/6JOlaHsd mice on a test battery assessing sensorimotor, affective and cognitive behaviours: Implications for the study of genetically modified mice. *Behav Brain Res* 124(1):33–46.
8. Threlfell S, et al. (2010) Striatal muscarinic receptors promote activity dependence of dopamine transmission via distinct receptor subtypes on cholinergic interneurons in ventral versus dorsal striatum. *J Neurosci* 30(9):3398–3408.
9. Threlfell S, et al. (2012) Striatal dopamine release is triggered by synchronized activity in cholinergic interneurons. *Neuron* 75(1):58–64.
10. Senior SL, et al. (2008) Increased striatal dopamine release and hyperdopaminergic-like behaviour in mice lacking both alpha-synuclein and gamma-synuclein. *Eur J Neurosci* 27(4):947–957.
11. Miles PR, Mundorf ML, Wightman RM (2002) Release and uptake of catecholamines in the bed nucleus of the stria terminalis measured in the mouse brain slice. *Synapse* 44(3):188–197.
12. Jennings KA, Lesch KP, Sharp T, Cragg SJ (2010) Non-linear relationship between 5-HT transporter gene expression and frequency sensitivity of 5-HT signals. *J Neurochem* 115(4):965–973.
13. Threlfell S, et al. (2004) Histamine H3 receptors inhibit serotonin release in substantia nigra pars reticulata. *J Neurosci* 24(40):8704–8710.
14. Brown MT, Henny P, Bolam JP, Magill PJ (2009) Activity of neurochemically heterogeneous dopaminergic neurons in the substantia nigra during spontaneous and driven changes in brain state. *J Neurosci* 29(9):2915–2925.
15. Franklin KBJ, Paxinos G (2007) *The Mouse Brain in Stereotaxic Coordinates* (Academic, New York), 3rd Ed.
16. Bishop MW, et al. (2010) Hyperexcitable substantia nigra dopamine neurons in PINK1- and HtrA2/Omi-deficient mice. *J Neurophysiol* 104(6):3009–3020.
17. Tepper JM, Martin LP, Anderson DR (1995) GABAA receptor-mediated inhibition of rat substantia nigra dopaminergic neurons by pars reticulata projection neurons. *J Neurosci* 15(4):3092–3103.
18. Paladini CA, Tepper JM (1999) GABA(A) and GABA(B) antagonists differentially affect the firing pattern of substantia nigra dopaminergic neurons in vivo. *Synapse* 32(3): 165–176.

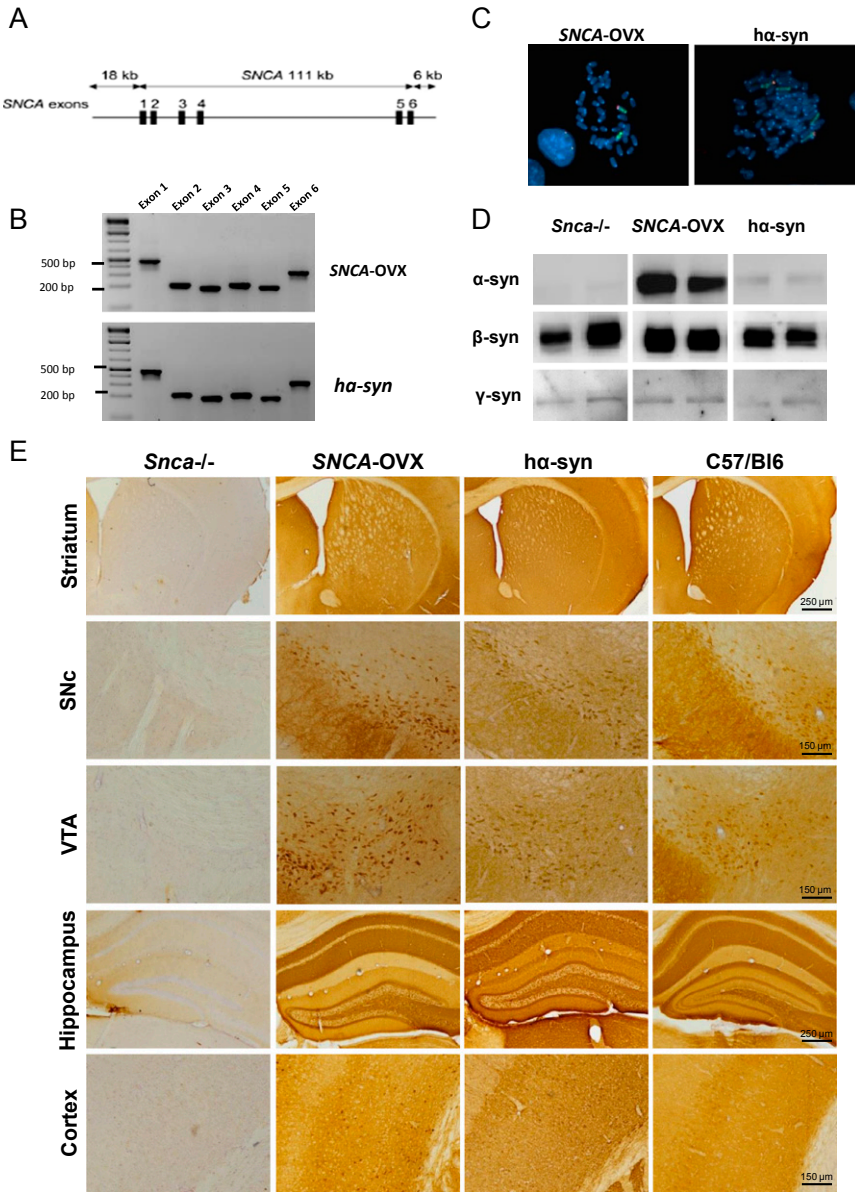

Fig. S1. Generation and characterization of human *SNCA* transgene expression. (*A*) Schematic representation of the BAC construct carrying the complete 111-kb human wild-type *SNCA* locus. (*B*) Exon PCR confirmed the full integration of the human *SNCA* BAC transgene in both *SNCA*-OVX and hα-syn transgenic mouse lines. (*C*) A single site of integration was confirmed for both transgenic mouse lines. Transgene integration in the *SNCA*-OVX line was observed close to the centromere on one copy of chromosome 4 and close to the telomere on one copy of chromosome 2 in the hα-syn line. (*D*) Quantitative Western blot analysis did not identify a change in the total levels of β- or γ-synuclein in *SNCA*-OVX mice. Representative blots are shown, $n = 3$ per genotype. (*E*) *SNCA* transgene expression was confirmed by immunohistochemistry (IHC) in 3-mo-old *SNCA*-OVX and hα-syn mice in regions including the striatum, SNc, ventral tegmental area (VTA), hippocampus, and cortex mirroring the expression pattern of endogenous *Snca* in C57/Bl6 mice. No α-syn expression was detected in $Snca^{-/-}$ mice. Representative images are shown.

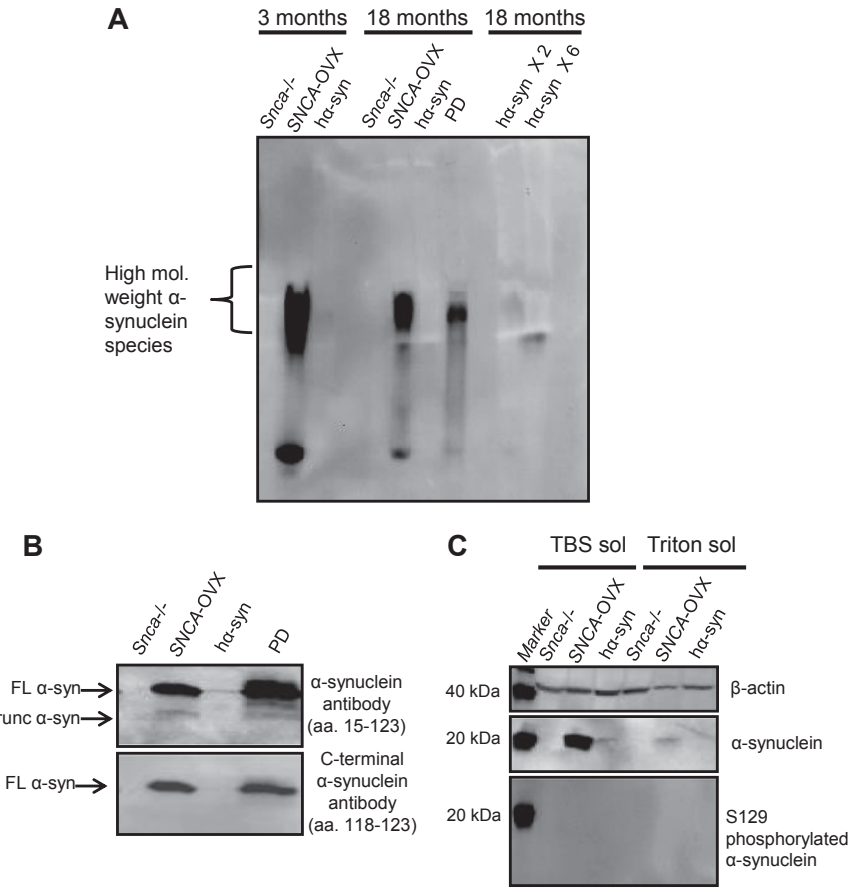

Fig. S2. Identification of modified and aggregated α-syn species in *SNCA*-OVX mice. (*A*) Overexpression of human wild-type α-syn results in formation of soluble high-molecular-weight species in both 3- and 18-mo-old *SNCA*-OVX mice at comparable high molecular weights to those observed in the SNc of a PD patient, as assessed by Western blot analysis. Representative blot of Triton-soluble midbrain extracts (25 μg) separated by native-PAGE is shown. (*B*) C-terminal truncation of human α-syn, in the midbrain of 18-mo-old *SNCA*-OVX mice and in the SNc of a PD patient. Representative blots using an antibody raised against aa 15–123 of human α-syn and an antibody recognizing a C-terminal epitope at aa 118–123 are shown. (*C*) Representative Western blot showing no evidence of S129 phosphorylation of α-syn in the midbrain of 18-mo-old *SNCA*-OVX mice in either the Tris-buffered saline-soluble or Triton-soluble fractions. Equal loading was confirmed by reprobing with β-actin and α-syn expression was confirmed using an α-syn antibody.

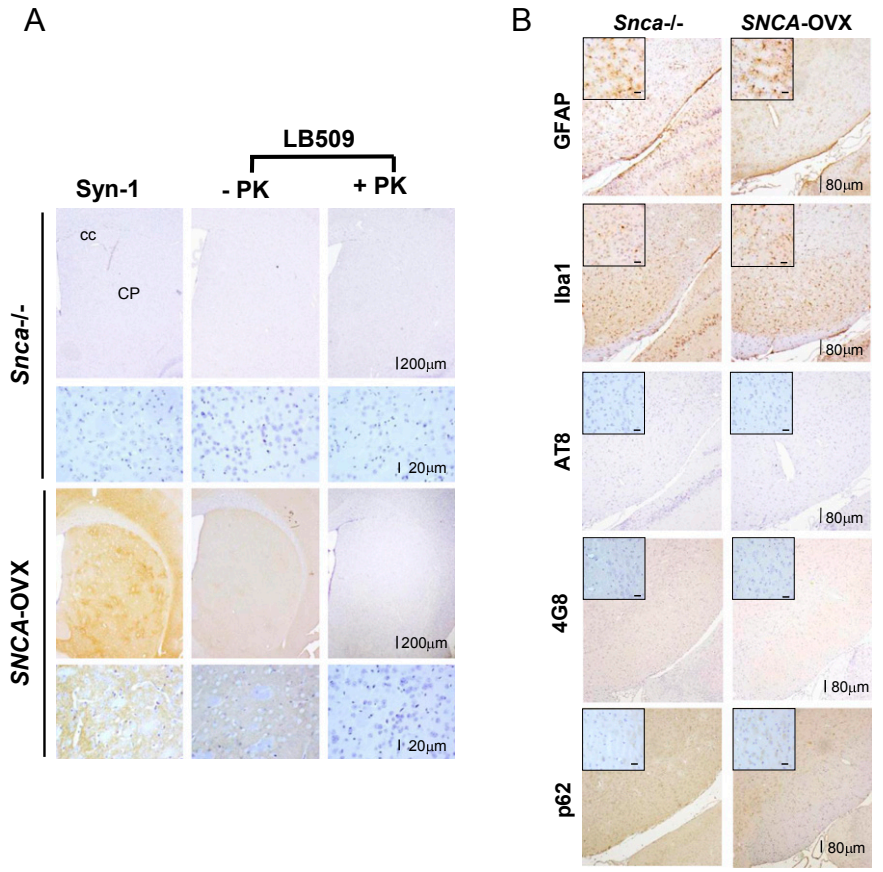

Fig. S3. Absence of neuropathology in 18-mo old *SNCA*-OVX animals. (*A*) Immunohistochemical analysis revealed diffuse α-syn immunostaining in the striatum of 18-mo-old *SNCA*-OVX mice using the Syn-1 antibody. Similar staining was weakly detected in 18-mo-old *SNCA*-OVX mice using the LB509 antibody (−PK). This staining was abolished when proteinase K antigen retrieval was applied (+PK). [Scale bars, 200 μm (Magnification: 40×) and 20 μm (Magnification: 400×)]. (*B*) We could not detect any qualitative differences in astrogliosis or microglial activation in SNc between genotypes as detected by GFAP or Iba-1 IHC staining, respectively. Hyperphosphorylated tau (AT8) and β-amyloid (4G8) staining was negative in all animals. Similarly, p62, a common constituent in several types of disease-associated inclusions, revealed no pathological protein aggregations in the SNc of *SNCA*-OVX mice. [Scale bars, 80 μm (Magnification: 100×); scale bars in inserts, 20 μm (Magnification: 400×)].

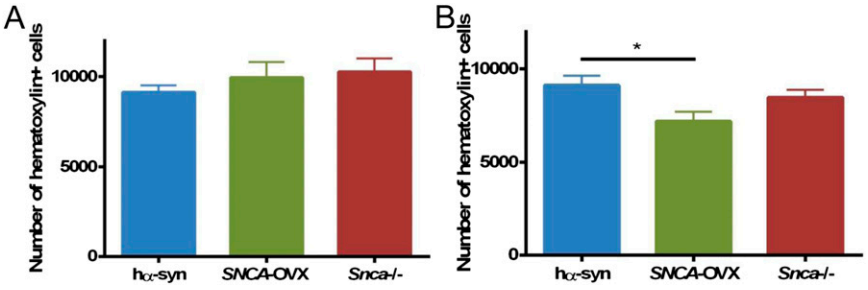

Fig. S4. *SNCA*-OVX mice show reduction in hematoxylin-positive neuron number in SNc at 18 mo of age. (*A*) At 3 mo of age, stereological cell counting revealed no differences in the number of hematoxylin-positive cells in the SNc of *SNCA*-OVX mice compared with hα-syn and *Snca*$^{-/-}$ mice (one-way ANOVA; no main effect of genotype: $F < 1$, $P > 0.05$, $n = 5$ per genotype). Data are expressed as mean ± SEM. (*B*) Analysis of 18-mo-old animals revealed a 22% loss of hematoxylin-immunoreactive neurons in the SNc of *SNCA*-OVX mice compared with hα-syn mice (one-way ANOVA with Bonferroni post hoc analysis; main effect of genotype: $F_{(2,12)} = 4.3$, $^*P < 0.05$, $n = 5$ per genotype). Data are expressed as the mean ± SEM.

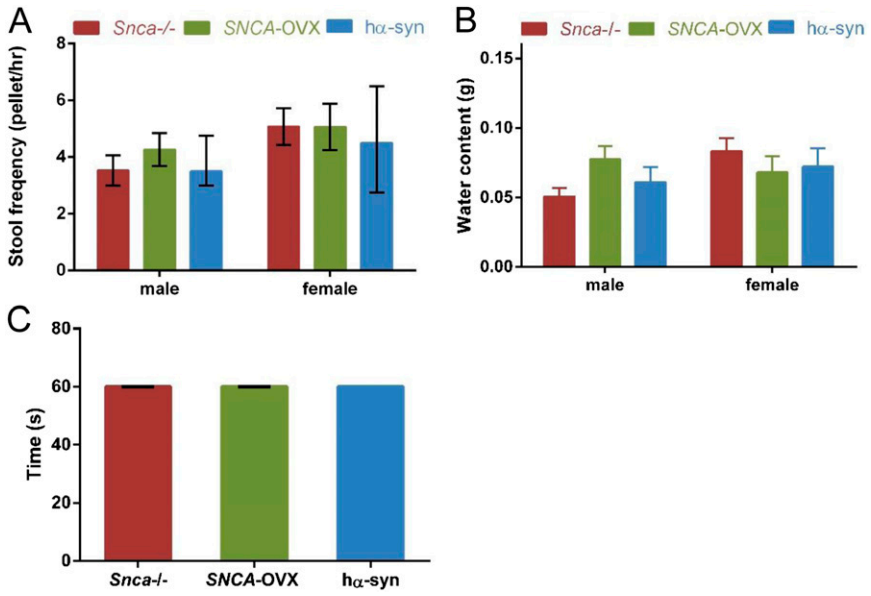

Fig. S5. *SNCA*-OVX mice do not display changes in stool frequency, stool water content, or muscle strength. (*A*) *SNCA*-OVX animals do not display changes in stool frequency at 3 or 18 mo of age. Data were combined for male and female mice and were subjected to a Kruskal–Wallis one-way ANOVA on the ranked data. There was no significant effect of genotype ($H < 1$; $P > 0.05$). Separate analyses for males ($H < 1$; $P > 0.05$) and females (parametric ANOVA; $F < 1$; $P > 0.05$) also showed no genotype effects. Data are expressed as median ± IQ range. (*B*) *SNCA*-OVX animals do not display changes in stool water content at 3 or 18 mo of age. Data were combined for male and female mice, and becayse assumptions were satisfied a parametric one-way ANOVA was performed. There was no significant effect of genotype ($F < 1$; $P > 0.05$). Separate analyses for males and females also showed no group differences. Data are expressed as mean ± SEM. (*C*) *SNCA*-OVX animals do not display changes in inverted screen performance at 18 mo of age. The majority of mice were able to hang on to the screen for 60 s (the maximum duration of the test). These data were analyzed using a Kruskal–Wallis test and there was no significant effect of genotype ($H < 1$; $P > 0.05$; $n = 7–10$). Data are expressed as median ± IQ range.

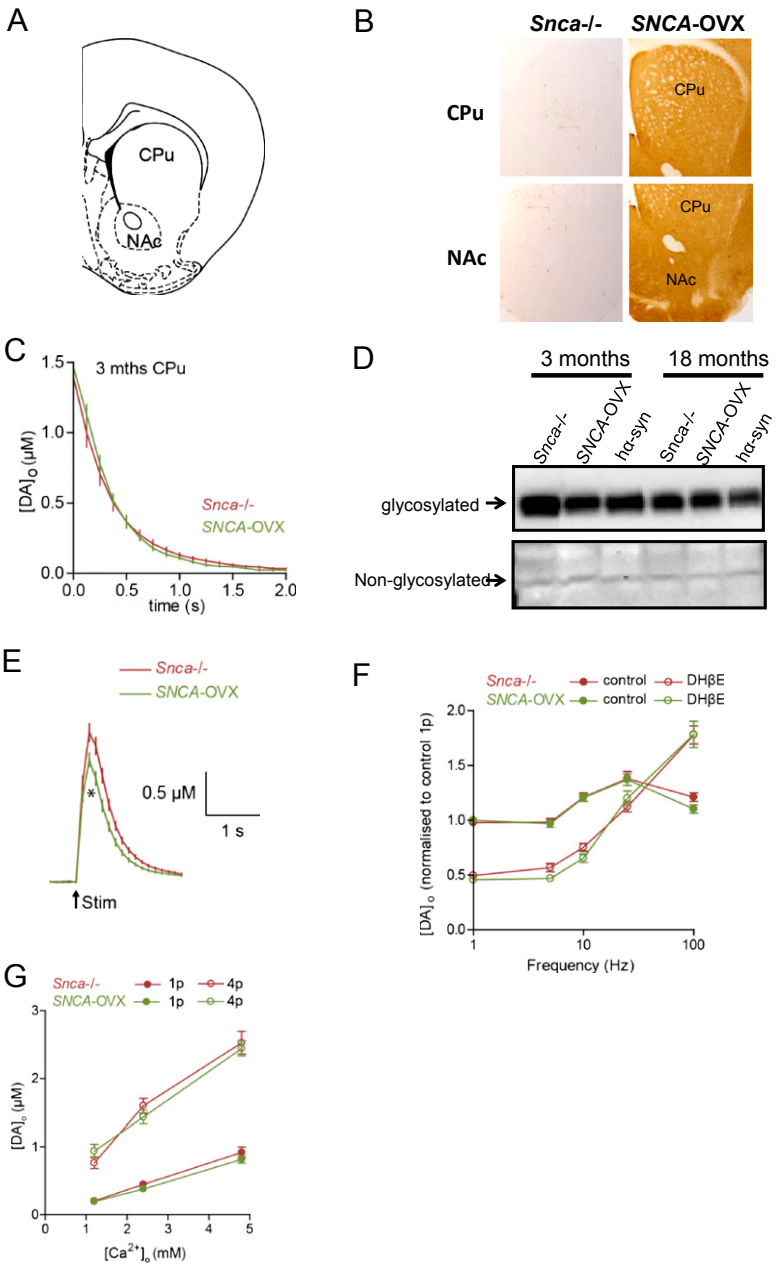

Fig. S6. Regulation of dopamine signaling by uptake, cholinergic input, and calcium are similar in the CPu of *Snca*$^{-/-}$ and *SNCA*-OVX mice. (*A*) Schematic highlighting a typical coronal slice used in dopamine release voltammetric recordings from dorsal striatum (CPu) and NAc. (*B*) Human α-syn transgene expression was confirmed in the CPu and NAc of 3-mo-old *SNCA*-OVX animals by immunohistochemical analysis. No immunoreactivity was detected in *Snca*$^{-/-}$ control animals. Representative images are shown. (*C*) Comparison of falling phases of mean dopamine release transients from CPu of 3-mo-old *Snca*$^{-/-}$ and *SNCA*-OVX mice reveals no significant difference (one-phase exponential decay curve fits; $P > 0.05$, $n = 60$, $R^2 > 0.85$; K = 2.798s^{-1} *Snca*$^{-/-}$ K = 2.79 s^{-1} *SNCA*-OVX). (*D*) No change in dopamine transporter expression was observed in *SNCA*-OVX mice. Representative blots of striatal lysates (25 μg) from 3- and 18-mo-old mice probed with an N-terminal dopamine transporter antibody are shown. (*E*) Mean profile of extracellular concentration of dopamine ([dopamine]$_o$) vs. time (mean ± SEM) following single-pulse stimulation (↑200 μs, 0.6 mA) in the CPu of *Snca*$^{-/-}$ vs. *SNCA*-OVX mice at 3–4 mo in the presence of nicotinic receptor blocker DHβE (1 μM). Mean peak evoked [dopamine]$_o$ was significantly lower in *SNCA*-OVX mice compared with *Snca*$^{-/-}$ in CPu (*$P < 0.05$; unpaired *t* test; n =54). (*F*) Mean peak [dopamine]$_o$ ± SEM vs. frequency during four pulse trains (1–100 Hz) in the dorsal striatum of *Snca*$^{-/-}$ and *SNCA* OVX mice at 3–4 mo, with and without inhibition of nicotinic acetylcholine receptors (nAChRs) (using DHβE). Data are normalized to [dopamine]$_o$ under control conditions. DHβE significantly altered mean peak [dopamine]$_o$ within each genotype in a frequency-dependent manner (***$P < 0.001$, two-way ANOVA; **$P < 0.01$, ***$P <$ 0.001 post hoc Bonferroni tests control vs. DHβE within genotype; three animals per genotype), but mean peak [dopamine]$_o$ was not significantly different between genotypes within a given condition ($P > 0.05$ post hoc Bonferroni tests *Snca*$^{-/-}$ vs. *SNCA*-OVX for a given drug condition; three animals per genotype). (*G*) Response of mean peak [dopamine]$_o$ evoked by a single pulse or four pulses at 100 Hz to varying extracellular calcium concentrations (1.2–2.4 mM) in CPu (in the presence of DHβE) did not significantly differ between genotypes at 3–4 mo ($P > 0.05$, two-way ANOVA with post hoc Bonferroni tests; three animals per genotype).

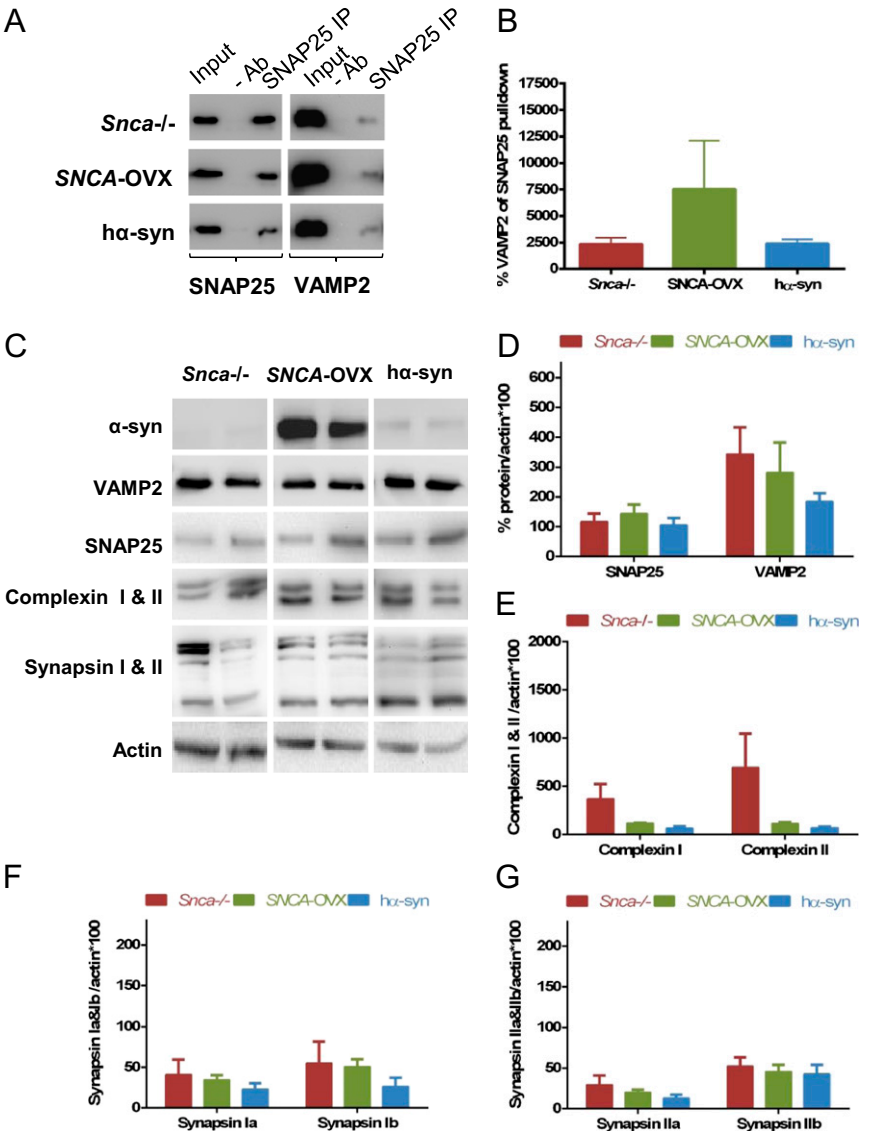

Fig. S7. *SNCA*-OVX mice do not display changes in SNARE complex formation. (*A* and *B*) At 6 mo of age, coimmunoprecipitation of SNAP25 with VAMP2 followed by quantitative Western blot analysis did not reveal changes in SNARE complex formation in *SNCA*-OVX mice. (*C* and *D*) Similarly, at 6 mo of age, no changes in the total striatal protein levels of the SNARE proteins VAMP2/synaptobrevin and SNAP25 were detected. In addition, no changes were found in the total striatal levels of the synaptic proteins (*C* and *E*) complexin I and II and (*C*, *F*, and *G*) synapsin I and II. Data represent average protein expression normalized to actin for three animals per genotype ± SEM. Three independent experiments were carried out.

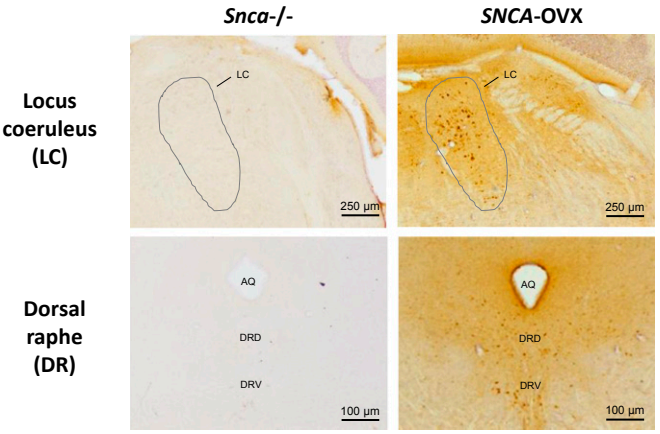

Fig. S8. Expression of α-syn transgene in locus coeruleus and dorsal raphe of *SNCA*-OVX mice. Human α-syn transgene expression was confirmed in locus coeruleus (LC) and dorsal raphe (DR) of 3-mo-old *SNCA*-OVX animals by immunohistochemical analysis. No immunoreactivity was detected in $Snca^{-/-}$ control animals. Representative images are shown. Aq, aqueduct; DRD, dorsal subdivision of dorsal raphe; DRV, ventral subdivision of dorsal raphe.

Table S1. Analyses of TH-positive structures in the dorsal striatum of 3-mo-old *SNCA*-OVX mice

Profiles	$Snca^{-/-}$, mean ± SEM	*SNCA-OVX*, mean ± SEM	*P* value, Mann–Whitney *U*
All profiles (150 profiles per genotype; $n = 3$)			
Cross-sectional area, μm^2	0.12 ± 0.02	0.10 ± 0.01	>0.05
Vesicles (per profile)	9.35 ± 0.85	8.82 ± 0.98	>0.05
Vesicle density, μm^2	81.28 ± 7.76	85.75 ± 6.23	>0.05
Vesicle distance to plasma membrane, nm	49.66 ± 5.83	45.32 ± 0.57	>0.05
Intervesicle distance, nm	375.79 ± 70.69	264.97 ± 8.49	>0.05
Profiles with synaptic specialization (33 profiles *SNCA-OVX*; 29 profiles $Snca^{-/-}$; $n = 3$)			
Cross-sectional area, μm^2	0.13 ± 0.04	0.11 ± 0.02	>0.05
Vesicles (per profile)	16.50 ± 3.10	14.53 ± 0.98	>0.05
Vesicle density, μm^2	135.57 ± 20.88	138.37 ± 22.93	>0.05
Vesicle distance to plasma membrane, nm	48.80 ± 5.28	43.41 ± 2.79	>0.05
Intervesicle distance, nm	302.12 ± 81.72	367.63 ± 64.26	>0.05
Synaptic membrane length, μm	0.11 ± 0.02	0.15 ± 0.03	>0.05
Distance to active zone, nm	240.62 ± 66.68	245.17 ± 57.74	>0.05

Table S2. Primary antibodies for Western blot analysis

Antibody	Host species	Dilution	Supplier and catalog number
Alpha-synuclein	Mouse (monoclonal)	1:1,000	Abcam, Ab1904 (Covance, SIG-39730)
Alpha-synuclein	Mouse (monoclonal)	1:1,000	BD Bioscience, 610786
Tyrosine hydroxylase	Rabbit (polyclonal)	1:1,000	Millipore, Ab152
Dopamine transporter	Rat (monoclonal)	1:5,000	Millipore, MAB369
SNAP-25	Mouse (monoclonal)	1:2,000	BD Transduction Labs, 610366
VAMP2	Rabbit (polyclonal)	1:1,000	Sigma, V1389
Complexin I and II	Rabbit (polyclonal)	1:1,000	Synaptic Systems, 122 002
Synapsin I and II	Guinea pig (polyclonal)	1:1,000	Synaptic Systems, 106 004
Beta-actin	Rabbit	1:2,000	Abcam, Ab8227

Movie S1. *SNCA*-OVX mice exhibit increased foot slips in multiple static rods test. Representative video of an 18-mo-old *SNCA*-OVX transgenic animal displaying increased foot slips and reduced motor coordination while traversing the rod (rod 2; 9 mm in diameter) during the multiple static rod test.

Movie S1

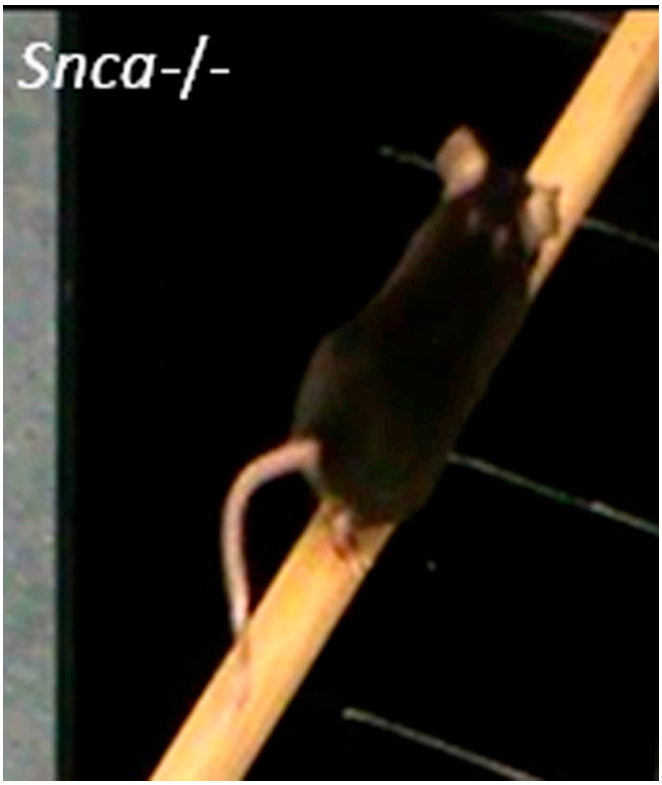

Movie S2. *Snca*$^{-/-}$ control mice show normal motor coordination in multiple static rods test. Representative video of an 18-mo-old *Snca*$^{-/-}$ control animal displaying absence of foot slips and normal motor coordination while traversing the rod (rod 2; 9 mm in diameter) during the multiple static rod test.

Movie S2